Light harvesting with Earth abundant *d*-block metals: development of sensitizers in dye-sensitized solar cells (DSCs)

Biljana Bozic-Weber, Edwin C. Constable* and Catherine E. Housecroft

Department of Chemistry, University of Basel, Spitalstrasse 51, CH4056 Basel, Switzerland

edwin.constable@unibas.ch
Phone: +41 61 267 1008

Abstract

Chemistry is facing the challenge of delivering new materials for energy harvesting and management. The development of a materials chemistry in which scarce elements are replaced by more abundant and sustainable materials is crucial to the commercial and societal acceptance of these new technologies. This review surveys the use of complexes of Earth abundant metals from the first row of the d-block as photosensitizers in dye-sensitized solar cells (DSCs), an emerging technology for solar light harvesting in which state-of-the-art devices currently use ruthenium or other platinum group metal complexes as photosensitizers.

Keywords

Dye-sensitized solar cells; metal complex; sensitizer; redox-mediator; solar energy conversion

Abbreviations

AM	Air mass
bpy	2,2'-bipyridine
DFT	Density functional theory
DSC	Dye-sensitized solar cell
ff	Fill factor
FTO	Fluorine-doped tin oxide
HOMO	Highest occupied molecular orbital
I_{sc}	Short circuit current (short circuit photocurrent)
IPCE	Incident photon to current efficiency (Incident photon to charge carrier efficiency)
IQE	Internal quantum efficiency
ITO	Indium tin oxide
IVT	Intervalence transfer

J_{sc}	Short circuit current density (short circuit photocurrent density)
LLCT	Ligand-to-ligand charge transfer
LUMO	Lowest unoccupied molecular orbital
MLCT	Metal-to-ligand charge transfer
MPCT	Metal-to-particle charge transfer
NHE	Normal hydrogen electrode
PGM	Platinum group metal
P_{max}	Maximum power
phen	1,10-phenanthroline
SCE	Saturated calomel electrode
TCO	Transparent conducting oxide
TDDFT	Time-dependent density functional theory
tpy	2,2':6',2''-terpyridine
V_{oc}	Open circuit voltage

1. Introduction

1.1 General background

The European Union in its *Energy Roadmap 2050* plans to cut greenhouse gas emissions by 80-95% by 2050.[1] Envisaged within this roadmap are approaches based on high energy efficiency, diversified supply technologies, high utilization of renewable energy sources, delayed carbon capture and storage and low nuclear deployment. All of these contributions to the overall strategy rely upon innovation in materials chemistry and materials science delivering new and efficient technologies in this time period.

Materials science and materials chemistry will play a critical rôle in the implementation of these ambitious strategic aims. Future strategies for utilising non-fossil energy sources have to address not only the efficiency of the processes but also assess their environmental impact and the sustainability of the underlying materials chemistry.

In the past quarter of a century, huge advances have been made in the design of smart materials for applications as diverse as molecular electronics, single molecule computing, lighting technology and solar energy harvesting. However, in many cases these advances are still either at the proof-of-concept stage or being deployed as first generation technology. These advances have been made with the imperative of establishing viability and demonstrating innovation and most commonly without constraints on materials cost or sustainability. For mass uptake, the new materials must be environmentally benign in the life-cycle and in the end-of-duty phase and must also be "sustainable". The latter constraint refers both to material availability and to the environmental acceptability of the primary processing steps. In energy

applications, the pay-back time calculated in financial or energy terms is also a critical factor

One of the highlights of innovative materials design is the dye sensitized solar cell (DSC) also known as the Grätzel cell. Conventional Grätzel DSCs (see the next section) function using ruthenium- or other platinum group metal- (PGM)-based photosensitizers to harvest photons [2]. Ruthenium is rare on the planet Earth and occurs native with the other PGMs osmium, rhodium, iridium, palladium and platinum. An overview of the abundance of elements in the Earth's crust is given in Figure 1. Estimated world resources [3] of elements are continually reassessed to account for newly discovered sources and changes in extraction technologies. For example, in 1970, world reserves of copper were estimated to be 280 Mt but this estimate had risen to 690 Mt in 2011. Nevertheless, Figure 1 provides a clear impetus for the design of materials for mass markets based upon the Earth abundant d-block metals of the first row rather than the PGMs.

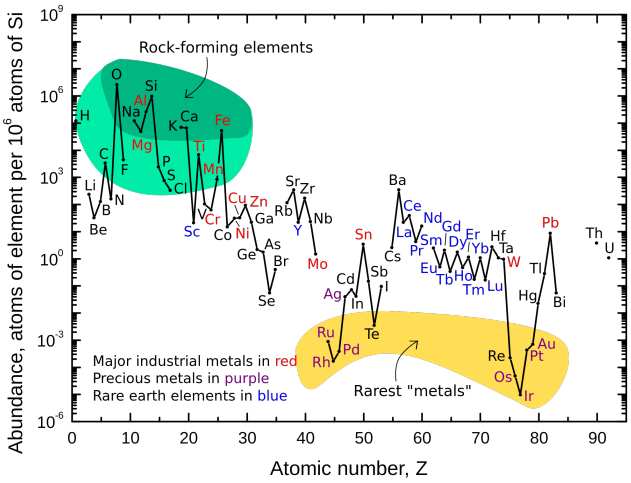

Fig. 1. Abundance of elements in the upper continental crust of the Earth normalized to an abundance of silicon of 10^6 (graphic courtesy of Wikimedia Commons) [4].

As seen in Figure 2, there is a near exponential growth in publications dealing with dye sensitized solar cells and this review concentrates upon the use of complexes of the first row d-block elements as photosensitizers in DSCs. Although a few porphyrinato and phthalocyaninato complexes are described in this article, we have generally excluded detailed coverage of these compounds as they have been extensively reviewed elsewhere [5,6,7,8], as have organic dyes [9]. We have

purposely not included artificial photosynthesis and water-splitting in this review; these topics have been adequately covered in other reviews [10,11,12,13,14,15].

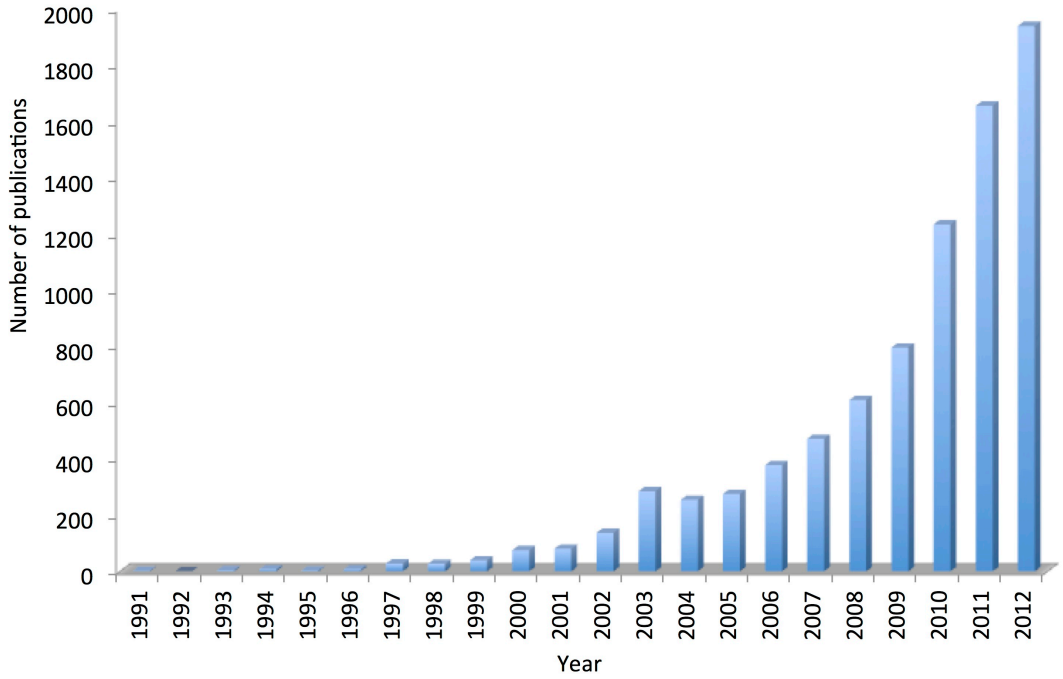

Fig. 2. Number of publications annually dealing with dye sensitized solar cells showing the near exponential growth in interest in recent years (Data collected from from Web of Science, 24.3.2013)

1.2 The dye sensitized solar cell

The Grätzel-type DSC was first developed in the early 1990s and converts solar energy to electrical energy using an optically transparent, wide-band gap semiconductor modified with a surface-bound inorganic dye (the *sensitizer*) that absorbs photons [16,17,18]. A schematic representation of the DSC is shown in Figure 3.

Visible light cannot excite an electron from the valence to the conduction band of a wide-band gap semiconductor such as TiO_2. In a DSC, the surface of the semiconductor is functionalized with a colored material, the *photosensitizer (dye*, Figure 3), that absorbs in the visible region and which has a ground state below and an excited state above the conduction band [19]. By using semiconductor nanoparticles, a very large functionalized surface area is associated with a small total device area. The electrons in the conduction band are harvested at a transparent

conducting oxide electrode (usually FTO or ITO). The oxidized photosensitizer is reduced to the ground state by an electrolyte hole transporter, archetypically composed of I^-/I_3^-. The circuit is completed by the catalytic reduction of I_3^- at a platinized counter-electrode. The efficiency of the cell is affected by many parameters which will be discussed where appropriate in the text of this review.

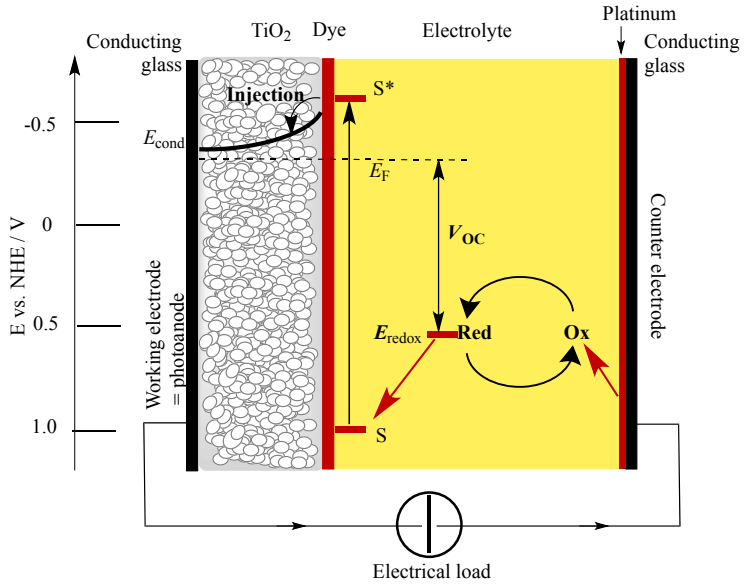

Fig. 3. Schematic representation of a dye-sensitized solar cell (DSC). E_F = Fermi level; E_{cond} = conduction band.

A correlation between photon flux of the Sun (AM 1.5 G spectrum at 100 mW cm^{-2}, AM = air mass) and calculated accumulated photocurrent [20] shows that a theoretical photocurrent density of 33 mA cm^{-2} could be obtained from a dye with an absorption threshold of 900 nm. The N3 dye (Scheme 1) absorbs light up to about 800 nm, while the absorption of the black dye (Scheme 1) extends to near 900 nm and gives a photocurrent density of 21 mA cm^{-2}. The incident photon to current efficiency (IPCE) values are close to 80% for wavelengths <650 nm for both sensitizers, but due to a relatively low molar extinction coefficients, they tail off at longer wavelengths (650–750 nm) resulting in a significant loss of photocurrent. Thus, improving the solar light absorption between 650 and 950 nm and decreasing the dye's optical band-gap will significantly increase efficiency. The voltage generated under illumination (V_{OC}) is the difference between the redox potential of the electrolyte (E_{redox}) and the Fermi level (E_F) of the mesoporous TiO_2 layer (Figure 3). At open circuit, the rates of electron injection and recombination/interception are equal, and their values determine the steady-state electron concentration in the semiconductor and therefore

its quasi-Fermi level. The band-gap of the dye is a critical factor in determining the value of V_{OC}, and for typical ruthenium(II) dyes attached to the TiO_2 surface, has a value of around 1.6 eV [21,22]. Cells which show good efficiency have a good compatibility between E_{redox} (Figure 3) and the HOMO level of the dye, and between the energy level of the conduction band (E_{cond}) of the semiconductor (Figure 3) and the LUMO of the dye.

The fill factor (*ff*) can possess values between 0 and 1 and is defined by the ratio of the maximum power (P_{max}) of the solar cell divided by the open-circuit voltage (V_{OC}) and the short circuit current (I_{SC}). The value of P_{max} is a consequence of the photocurrent and photovoltage at the voltage where the power output of the cell is at a maximum. The value of *ff* reflects electrical and electrochemical losses occurring during operation of the DSC. The overall solar conversion efficiency, η, is a function of the short-circuit current density (J_{SC}), V_{OC} and *ff* (eq. 1 in which P_{IN} is the total solar power incident on the cell, 100 mW cm^{-2} for air mass 1.5).

$$\eta = \frac{J_{SC} V_{OC} ff}{P_{IN}} \qquad (1)$$

Scheme 1 shows the structures of selected ruthenium-based state-of-the-art dyes used in the currently best performing devices [23,24,25]. Their composition illustrates the key structural features required in a photosensitizer (Figure 4). Firstly, the compound must be colored! The color can arise from purely ligand-based transitions (as in porphyrin or phthalocyanine complexes) or from transitions with significant metal character in the ground or excited states (for example, MLCT or LMCT bands). Photosensitizers should harvest light over the maximum possible range of wavelengths (ideally over the entire visible part of the spectrum as well as the NIR). and with high extinction coefficients for the absorption bands. Naturally, the photosensitizers should be photostable when bound to the semiconductor. Secondly the photosensitizer should be covalently bonded to the semiconductor, with the favoured attachment being through carboxylic acid, phosphonic acid or phenol groups. In general, dyes should be selected such that aggregation phenomena at the surface are minimised. The third design feature in the use of ancillary ligands for the fine tuning of the absorption spectrum to optimize the photonic harvesting, and fine tuning of the redox potential of the dye for compatibility with the energy of the upper

edge of the valence bands of the semiconductor and with the redox couple of the electrolyte.

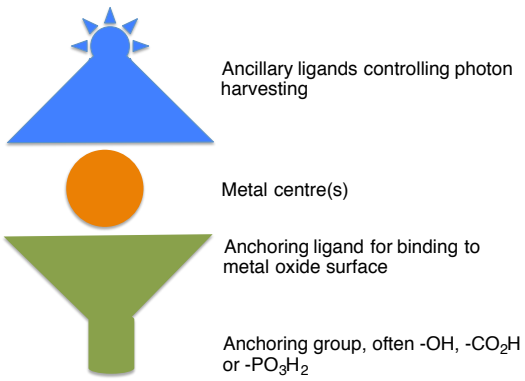

Fig. 4. The components of a typical metal-containing photosensitizer.

If we consider the electronic structures in more detail, Hagfeldt *et al.* in an excellent review have identified the factors which need to be taken into consideration in the design of ligands and complexes for use as photosensitizers in DSCs [26]. In particular they identify the following critical points that need to be built into the design: (i) for n-type semiconductors (e.g. TiO_2) the excited state level of the dye must be higher in energy than the conduction band to permit efficient electron transfer, (ii) the energy of the oxidized dye must be more positive than the redox potential of electrolyte, and (iii) for DSCs with p-type semiconductors (e.g. NiO), the HOMO of the dye should more positive than the valence band.

Since the performance of a DSC depends substantially upon the device fabrication, we have made a point in this review of stating electrode materials, electrolyte and additives and whether the cell is open (electrodes pressed together with electrolyte filling the gap) or sealed (electrodes sealed together and electrolyte injected through a drilled hole before the latter is sealed). In the former, the electrolyte is exposed to air, while in the latter it is not [27]. We note also the great importance of masking cells for consistency of performance in different experimental systems [28], although this is only slowly gaining recognition in the DSC community.

This review is based on the literature available through mid-March 2013.

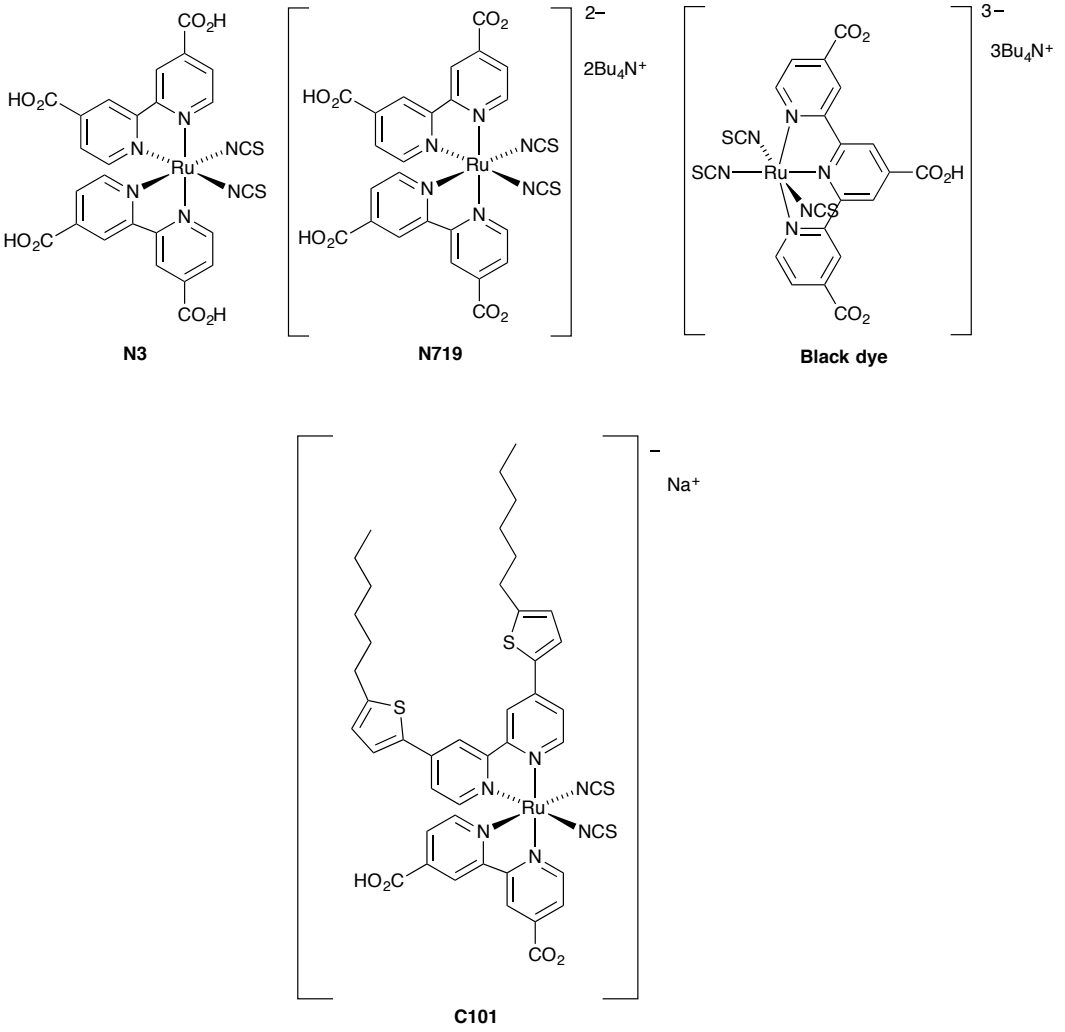

Scheme 1. The structures of selected ruthenium(II)-based dyes used in state-of-the-art DSCs; N3, N719, C101 and Black dye can exhibit efficiencies of >10%.

2 Systematic review of the use of Earth abundant metals in DSCs

2.1 Titanium

The development of nanoparticulate, mesoporous TiO_2 (anatase) as the semiconductor of choice in fabrication of photoanodes is outside the scope of this review, and we focus only on the very limited number of titanium complexes used as dyes in DSCs. Titanium(IV) complexes are usually colorless unless the ligands have chromophores that absorb in the visible region.

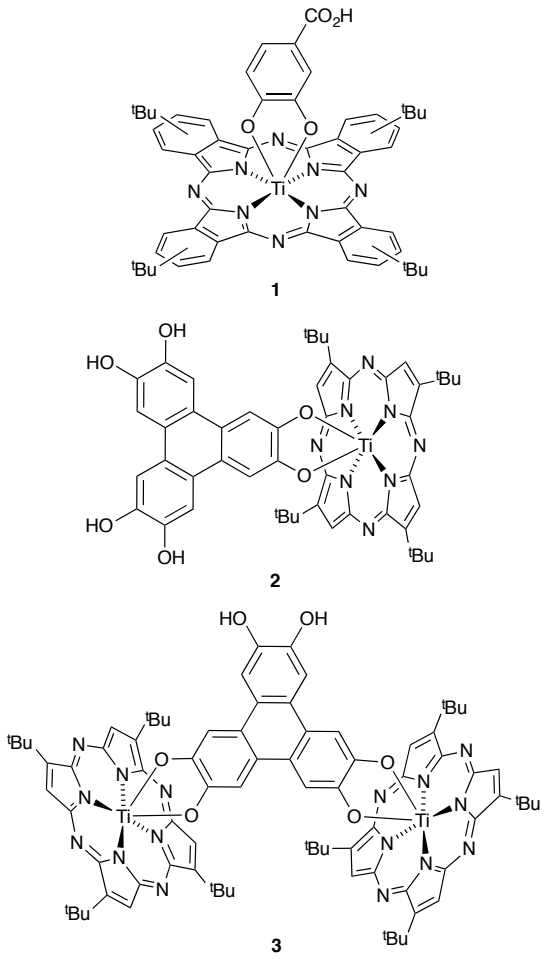

Scheme 2. Structures of the most promising titanium complexes investigated as dyes in DSCs.

Phthalocyanines exhibit a broad spectral response with intense absorptions in the ultraviolet (Soret band) and near infrared (Q band). A drawback to their use as sensitizers in DSCs is their tendency to aggregate through intermolecular π-interactions. Efforts focus on developing phthalocyanine-based dyes which minimize aggregation while maintaining a good energy match between the LUMO of the dye and the TiO_2 conduction band [29]. Compound **1** (a mixture of structural isomers, Scheme 2) combines the features of a phthalocyanine (solution absorption λ_{max} = 702 nm, ε = 135000 dm^3 mol^{-1} cm^{-1}) with a carboxylic acid anchoring functionality. The dye binds strongly to TiO_2 and spectroscopic data are consistent with negligible molecular aggregation on the surface. Efficient electron injection into the semiconductor conduction band and slow recombination are reported. The latter is consistent with adsorption through surface-binding by the carboxylic acid and the

phthalocyanine lying parallel to the TiO_2 surface; a dye-surface separation of 12 Å has been estimated from theoretical data. State selective electron injection occurs; efficient charge separation follows Soret band excitation, while excitation into the Q-band results in poor charge separation. IPCE data for the dye in the DSC device configuration show efficient and low photocurrent generation in the UV and near IR regions, respectively, and the overall efficiency of the device is only 0.2% [30]. Compound **1** has been included in a DFT/TDDFT study of a family of phthalocyanine and porphyrazine titanium(IV) complexes, screened *in silico* for their suitability as dyes in DSCs. The results indicate that the best candidates of those investigated, and which exhibit appropriate anchoring groups, are the porphyrazine analogs of **1** along with complexes **2** and **3** (Scheme 2) [31].

2.2 Vanadium and chromium

No DSCs functionalized with molecular vanadium- or chromium-containing chromophores appear to have been reported to date.

2.3 Manganese

Although the use of manganese complexes as photosensitizers in Grätzel-type DSCs is very limited, the metal plays an important role in biomimetic artificial photosynthesis. This area, particularly concerning the use of manganese-ruthenium conjugates, has been thoroughly reviewed elsewhere [[10],11,12].

Metalloporphyrins, in particular those containing zinc, show promise as sensitizers and offer an exciting new approach to DSCs [5]. The metalloporphyrins in Scheme 3a have been employed in sealed DSCs fabricated with TiO_2 and Pt as photoanode and cathode, respectively, and with I^-/I_3^- as electrolyte. The six complexes exhibit typical spectra with intense, high-energy Soret bands and weaker, lower energy Q bands. For the manganese complex, the Soret band is split (λ_{max} = 381, 426, 481 nm) as is characteristic of a manganese(III) porphyrin. Compared to an efficiency of 5.85% measured by the authors for the standard dye N3 (Scheme 1), the metalloporphyrins exhibit efficiencies of between 3.58% for M = Zn and ≤ 0.05% for M = Mn, Fe and Co. It is proposed that facile reduction of the latter metal ions inhibits electron injection into the semiconductor [32]. The performance of the manganese(III) porphyrin [Mn-HT-SCN] (Scheme 3b) has been compared with that of the

gallium(III) analog, [Ga-HT-SCN]. The absorption spectrum of [Mn-HT-SCN] is red-shifted with respect to that of [Ga-HT-SCN] and values of ε_{max} are higher for the manganese(III) complex. In the solar-cell device configuration (single layer TiO_2 on FTO photoanode, I^-/I_3^- electrolyte), [Mn-HT-SCN] performs moderately well exhibiting V_{oc} = 610 mV, J_{sc} = 4.32 mA cm^{-2}, *ff* = 0.58 and η = 1.53%; these values compare to V_{oc} = 650 mV, J_{sc} = 2.74 mA cm^{-2}, *ff* = 0.59 and η = 1.05% for [Ga-HT-SCN] [33]. Polymer photovoltaic cells incorporating manganese(II) phthalocyanine dyes have also been reported [34].

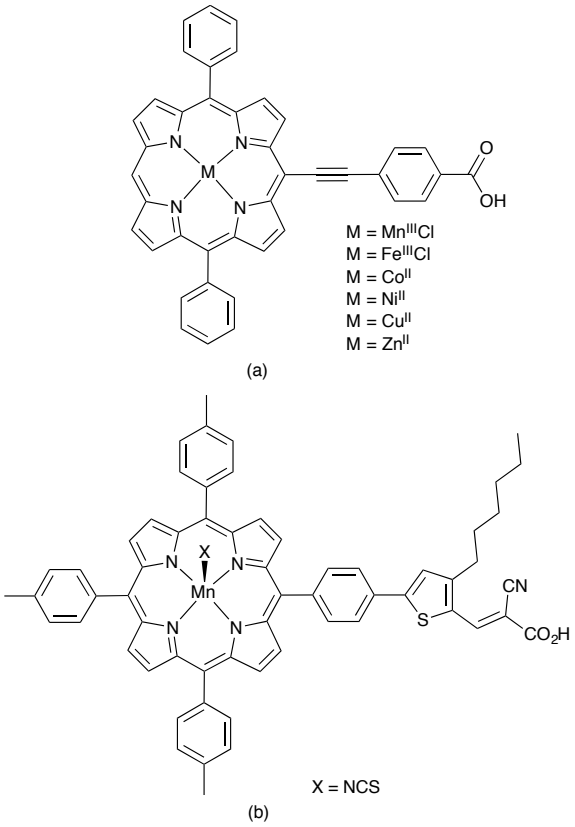

Scheme 3. (a) Metalloporphyrin dyes used in a study to investigate the effects of the central metal ion on the performance of the sensitizer in DSCs. (b) Structure of [Mn-HT-SCN].

The metalloporphyrin dyes in Scheme 3 possess carboxylic acid or cyanoacrylic acid anchoring groups, both of which are effective at binding to TiO_2 surfaces. The effectiveness of an anchoring group is dictated by a number of factors, two of the most critical of which are the mode of interaction between semiconductor and anchoring group, and the influence of the anchoring unit on the electronic structure of the dye [35]. Compared to the ubiquitous carboxylates and phosphonates,

hydroxamate anchors have been less commonly explored, but they show promise for functionalizing TiO_2 under aqueous conditions. Spectroscopic data are consistent with anchoring ligand **5** (Scheme 4) binding to TiO_2 nanoparticles through the hydroxamate unit. The tpy-domains bind manganese(II) when the functionalized surface is subsequently treated with $Mn(OAc)_2$; ESR spectroscopy has been used to confirm Mn^{2+}/Mn^{3+} reversible photooxidation, the latter demonstrating interfacial electron transfer between TiO_2 and metal center via the hydroxamate anchoring unit. Binding enthalpy data suggest that the hydroxamate–TiO_2 interaction is more stable than a carboxylate–TiO_2 anchor [36].

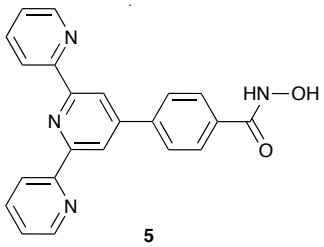

5

Scheme 4. Structure of 2,2':6',2"-terpyridine ligand **5** which contains a hydroxamate anchoring group.

2.4 Iron

Group 6 metal-containing sensitizers in DSCs have been dominated by those containing ruthenium(II) and to a lesser extent osmium(II). A review published in 2004 [37] indicated few examples of other d^6 metal-based dyes. Recently, X-ray absorption spectroscopy and DFT calculations have been used to probe the differences in the electronic structures of ruthenium(II) and iron(II)-based sensitizers. When the metal ion is octahedral, (e.g. $[M(bpy)_3]^{2+}$ or $[M(phen)_3]^{2+}$), the N 1s-to-π* transition moves to lower energy on going from Ru to Fe and there is a greater transfer of negative charge from metal to nitrogen donor atoms for M = Fe than for M = Ru; the 3d valence states of the dyes remain to be investigated [38].

The first example of the use of a simple iron complex as a photosensitizer in a DSC was reported in 1998, when $[Fe\{bpy\text{-}4,4'\text{-}(CO_2H)_2\}_2(CN)_2]$ (bpy-4,4'-$(CO_2H)_2$ = H_2**6**, Scheme 5) in the presence of chenodeoxycholic acid (cheno, **7**, Scheme 5) was shown to give functional devices with V_{oc} = 360 mV under 1 sun irradiation. The DSCs are blue and the complex has absorption maxima at 430 and 635 nm. The photocurrent

action spectrum indicates that injection from the higher energy band at 430 nm is much more efficient than from the lower energy band. Although electron injection is fast and estimated to occur in < 25 ps [39], the short MLCT lifetime means that internal non-radiative decay competes with electron transfer and the overall efficiency is relatively low [40]. These studies were subsequently extended to the complexes $[^nBu_4N]_4[Fe(\mathbf{6})_2(CN)_2]$, $[Fe\{bpy\text{-}4,4'\text{-}(CH_2OH)_2\}_2(CN)_2]$, $[Fe\{bpy\text{-}4,4'\text{-}(CH_2OH)_2\}_3]$, $[^nBu_4N]_4[Fe\{bpy\text{-}5,5'\text{-}(CO_2)_2\}_2(CN)_2]$ (bpy-5,5'-$(CO_2H)_2$ = $H_2\mathbf{8}$, Scheme 5), $[^nBu_4N]_8[Fe\{bpy\text{-}4,4'\text{-}(PO_3)_2\}_2(CN)_2]$, $[^nBu_4N]_8[Fe\{bpy\text{-}4,4'\text{-}(CH_2PO_3)_2\}_2(CN)_2]$, $[Fe\{bpy\text{-}4,4'\text{-}(PO_3Et_2)_2\}_2(CN)_2]$ and $[Fe\{bpy\text{-}4,4'\text{-}(CH_2PO_3Et_2)_2\}_2(CN)_2]$ [41,42]. Like $[Fe(bpy)_2(CN)_2]$ [43], the complexes are solvatochromic. Interesting structure-function relationships were derived relating the nature, position and protonation state of the substituents to the effectiveness of binding and the overall efficiency of the DSC. The complex $[Fe(4,4'\text{-}Me_2bpy)_2)(CN)_2]$ does not adsorb on TiO_2, eliminating speculation that the binding occurs through cyanido ligands or by reaction of surface hydroxide with cyanide. In contrast, theoretical and experimental studies of $[Fe(bpy)(CN)_4]^{2-}$, $[Fe(4,4'\text{-}Me_2bpy)(CN)_4]^{2-}$ and $[Fe(4,4'\text{-}Ph_2bpy)(CN)_4]^{2-}$ indicate that a direct interaction of the nitrile with the surface is critical in electron injection, consistent with the observation of two discrete charge transfer mechanisms, assigned to MLCT and MPCT pathways [44,45]. It is well established that $[Fe(CN)_6]^{4-}$ binds to TiO_2 through the cyanido ligands and that the observed Fe(II)→Ti(IV) IVT band at 420 nm provides evidence for efficient electron injection, probably through MPCT and MLCT pathways [44,46,47,48]. The mechanism of electron injection by ruthenium(II) polypyridyl complexes has been the subject of numerous studies, but is less well explored for iron(II) analogs. The complex $[Fe\{tren(py)_3\}]^{2+}$ ($tren(py)_3$ = **9**, Scheme 5) has been chosen for femtosecond time-resolved absorption measurements because of its spin crossover behaviour which renders it suitable for an investigation of excited-state dynamics. It was confirmed that excitation leads to the formation of a long-lived $^5T_2$ ligand-field state within 1 ps; the charge-transfer character of the initial excited state is lost in <100 fs as the ligand-field state forms. It was concluded that charge injection from iron(II) polypyridyl complexes into TiO_2 in a DSC occurs on an ultrafast timescale and suggested that charge injection may involve the initial excited state in addition to the long-lived state formed afterwards [49].

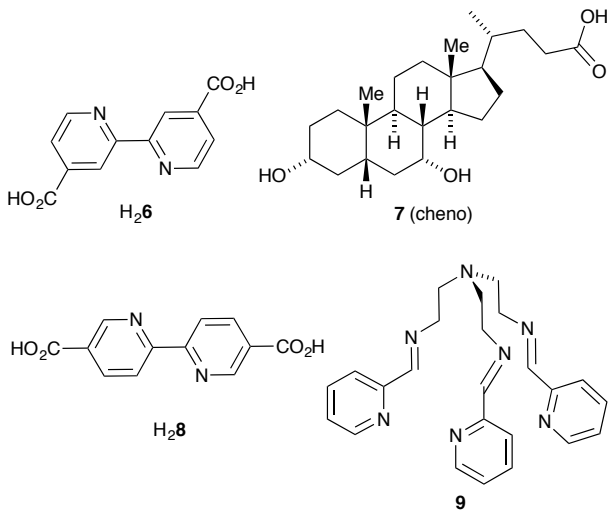

Scheme 5. Structures of chelating N-donor ligands used in iron(II) complexes and of the co-adsorbant, cheno.

The two metal-binding domains in *N*,*N*-bis(2,2':6',2"-terpyridinyl-4'-(4-phenyl))aniline, **10** (Scheme 6) are directed at 120° with respect to one another and a metallocyclic hexamer (Scheme 6) assembles when **10** reacts with $FeCl_2 \cdot 4H_2O$. Solution ^{1}H NMR spectroscopic data indicate the presence of one species and the electrospray mass spectrum of the $[PF_6]^-$ salt is consistent with retention of the hexamer. Acetonitrile solutions of $[Fe_6(\mathbf{10})_6][PF_6]_{12}$ absorb strongly in the UV and visible regions with the weakest absorption (the MLCT band at 423 nm) having a molar extinction coefficient of 177000 $dm^3\ mol^{-1}\ cm^{-1}$. This high absorption leads to $[Fe_6(\mathbf{10})_6][PF_6]_{12}$ being tested as a sensitizer in a DSC constructed from an ITO/TiO_2 photoanode, a Ti/colloidal graphite counter-electrode and I^-/I_3^- electrolyte. Performance of the cell was relatively poor (V_{OC} = 255 mV, J_{SC} = 0.16 mA cm^{-2}, *ff* = 0.269, η = 0.032%) but was improved by replacing Fe^{2+} by Zn^{2+}. For $[Zn_6(\mathbf{10})_6][PF_6]_{12}$, device characteristics were V_{OC} = 391 mV, J_{SC} = 0.23 mA cm^{-2}, *ff* = 0.681, η = 0.180% [50]. In this case, there is no formal anchoring group in the complex.

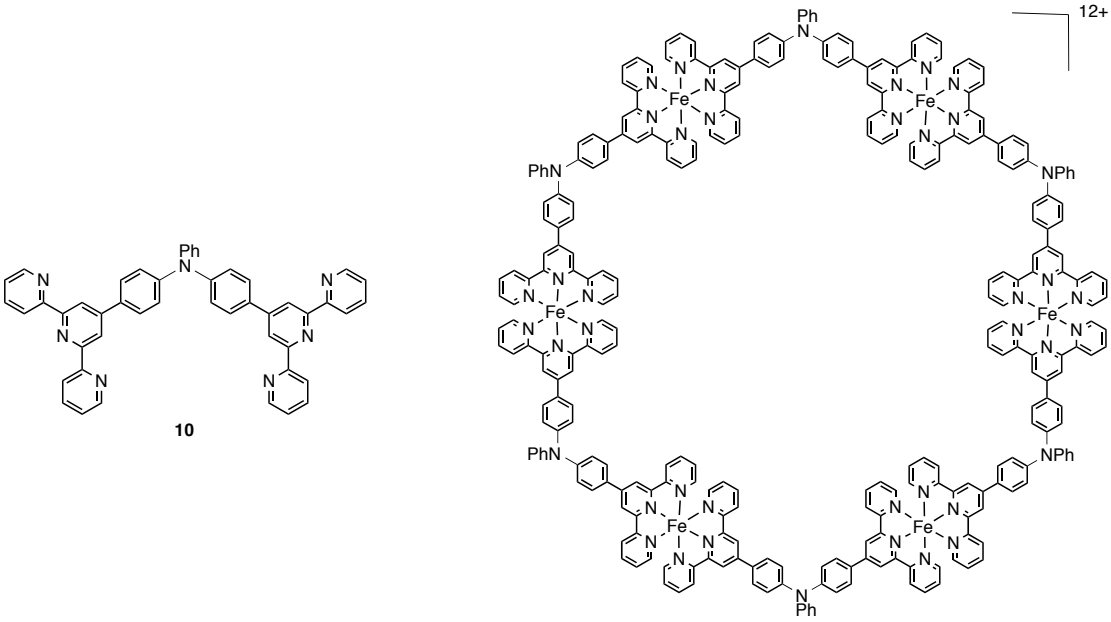

Scheme 6. Structures of ligand **10** and of the cation in $[Fe_6(\mathbf{10})_6][PF_6]_{12}$.

Recently, DFT calculations at various levels have been evaluated as a design tool for the investigation of a wide range of complexes with appropriate ground state electronic properties for use as photosensitizers in DSCs [51,52,53,54]. Additional insight has been gained through development of structure–property relationships based upon crystallographic data for salts of $[Ru(bpy)_n(\mathbf{6})_{3-n}]^{2+}$ (n = 0, 2, see Scheme 5 for $H_2\mathbf{6}$), $[Ru(bpy)_3]Cl_2{\cdot}6H_2O$ and $[Fe(bpy)_3][NCS]_2$. The absorption spectra of aqueous solutions of $[Fe(bpy)_3][NCS]_2$, $[Ru(bpy)_3]Cl_2{\cdot}6H_2O$, $[Ru(bpy)_2(\mathbf{6})][PF_6]_2$, $[Ru(\mathbf{6})_3]Cl_2$ have been evaluated with respect to that of standard dye N3 (Scheme 1) and DSC device efficiencies have been compared for sealed cells, each fabricated using an FTO/TiO_2 photoanode soaked in a solution of the respective dye, FTO/Pt counter-electrode, and I^-/I_3^- electrolyte. The results of this comparative study (using cells made under the same conditions and in one batch) are given in Table 1. The data are consistent with the anchoring groups being essential both for dye uptake and efficient electron injection [55]. Unfortunately, the only iron(II)-containing dye tested in this study did not have formal anchoring groups.

Table 1. Comparison of DSC performances using $[Fe(bpy)_3][NCS]_2$ and $[Ru(bpy)_n(\mathbf{6})_{3-n}]^{2+}$-based dyes versus N3. Data from reference [55].

Dye	V_{OC} / mV	J_{SC} / mA cm^{-2}	*ff*	η / %
N3	610	19.38	0.68	6.28
$[Fe(bpy)_3][NCS]_2$	450	0.56	0.50	0.13
$[Ru(bpy)_3]Cl_2{\cdot}6H_2O$	280	0.07	0.43	0.01
$[Ru(bpy)_2(\mathbf{6})][PF_6]_2$	430	7.53	0.67	0.95
$[Ru(\mathbf{6})_3]Cl_2$	600	7.53	0.69	1.96

Although iron-containing sensitizers are dominated by complexes containing polypyridyl ligands, a number of other iron(II) species have been investigated as sensitizers in DSCs. Aqueous solutions of bromopyrogallol red (**11**, Scheme 7) exhibit intense absorptions in the UV and visible regions (λ_{max} = 290, 440 and 540 nm). This, coupled with an ability to bind efficiently to TiO_2, makes bromopyrogallol red and related dyes of interest as sensitizers in DSCs [56,57,58]. Complexation of bromopyrogallol red to iron(II) red-shifts the absorption in the visible range. A combination of **11** and $[Fe(ox)_2(OH_2)_2]^{2-}$ (ox^{2-} = oxalate) has been tested as a sensitizer in DSCs constructed from a dye-sensitized TiO_2/conducting SnO_2 glass photoanode, I^-/I_3^- electrolyte and Pt/TCO counter-electrode. The dye was prepared by first collecting the precipitate from the reaction of oxalic acid with aqueous $Fe[NH_4]_2[SO_4]_2$ and then treating the resulting iron(II) complex with **11**. Characterization of the dye was limited to UV-VIS spectroscopy and cyclic voltammetry. With 750 W m^{-2} illumination, the DSC performed with characteristics of V_{OC} = 423 mV (cited in the original work as V cm^{-2}), J_{SC} = 1.23 mA cm^{-2} and η = 0.29, compared to characteristics of a cell using **11** alone as sensitizer of V_{OC} = 411 mV (cited in the original as V cm^{-2}), J_{SC} = 0.83 mA cm^{-2} and η = 0.20. Thus, complexation to iron(II) only modestly influences the performance of **11** in DSCs.

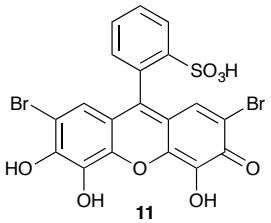

11

Scheme 7. The structure of bromopyrogallol red (**11**).

In DSCs, ferrocene is most often encountered as a redox mediator [24,59,60,61] although fast recombination of injected electrons with Fe^{3+} may offset the advantages of efficient reduction of the oxidized dye [62]. Recently, a number of reports have appeared in which functionalized ferrocenes have been utilized as sensitizers in DSCs. The electronic absorption spectra of CH_2Cl_2 solutions of the complexes shown in Scheme 8 exhibit bands around 450, 360, 300 and 250 nm and analogous nickel(II), copper(II) and cobalt(III) complexes absorb over the range 550–750 nm. Sealed DSCs were prepared by dipping TiO_2-coated electrodes into MeOH solutions of the dyes and combining each photoanode with a Pt-coated working electrode and I^-/I_3^- electrolyte. The DSCs were illuminated with visible light ($\lambda > 420$ nm) and their performances compared to that of a DSC with the standard dye N719 (Table 2). The nickel(II), copper(II) and platinum(II) complexes, each of which contains a square planar metal ion, appear to show remarkable potential reaching power conversion efficiencies over half that of N719 [63]. We note that these data must be treated with caution in view of the excessively low device performance of the standard N719 cell presented for comparison.

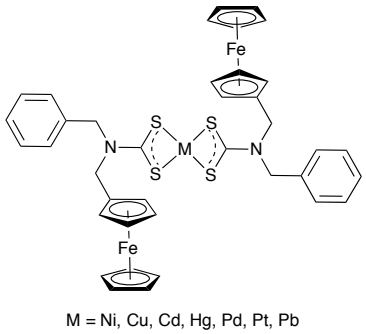

M = Ni, Cu, Cd, Hg, Pd, Pt, Pb

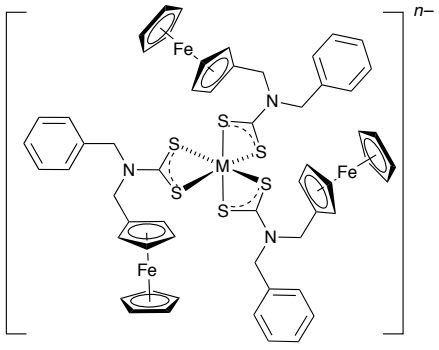

M = Co, n = 0; M = UO_2, n = 1

Scheme 8. Dithiocarbamate complexes $[ML_2]$, $[CoL_3]$ and $[UO_2L_3]^-$ containing pendant ferrocenyl units tested as sensitizers in DSCs.

Table 2. Comparison of DSC performances using dithiocarbamate complexes with pendant ferrocenyl units (Scheme 8) versus N719. The very low performance of the standard N719 cell should be noted. Data from reference [63]; light intensity was 470 mW cm^{-2}.

Dye (L^-, see Scheme 8)	V_{OC} / mV	J_{SC} / mA cm^{-2}	*ff*	η / %
N719	750	8.95	0.70	1.00
$[NiL_2]$	710	6.43	0.63	0.63
$[CuL_2]$	710	5.58	0.62	0.54
$[CdL_2]$	710	3.80	0.62	0.37
$[HgL_2]$	710	4.00	0.63	0.38
$[PdL_2]$	710	3.63	0.62	0.36
$[PtL_2]$	710	5.71	0.62	0.56
$[PbL_2]$	710	3.20	0.64	0.31
$[CoL_3]$	710	4.70	0.62	0.46
$[Et_3NH][UO_2L_3]$	710	4.40	0.64	0.43

Ferrocene is readily functionalized with anchoring groups as seen in derivatives **12–14** (Scheme 9). These compounds absorb between 440 and 480 nm as well as at higher energy (250, 300 and 360 nm); consideration of the lowest energy absorption and electrochemical properties indicated that **12–14** might be suitable as sensitizers. The latter have been screened in sealed DSCs each constructed with a TiO_2/conducting glass photoanode onto which the dye was absorbed (6 hour soaking period), a Pt-coated conducting glass counter electrode, and I^-/I_3^- electrolyte either with propylene carbonate or ionic liquid (1-propyl-3-methylimidazolium iodide). Compared to the standard dye N719, the ferrocenyl dyes perform well (Table 3) [64]. Related studies have focused on ferrocene derivatives **15–19** (Scheme 9) [65,66]. Compounds **15** and **16** absorb at 440 nm (characteristic of the ferrocene unit) and in the UV region, but molar extinction coefficients are rather low (<4000 dm^3 mol^{-1} cm^{-1}). From electronic absorption and cyclic voltammetric data, the energy levels for electron injection from the excited state dye molecules **15** and **16** are determined as –2.469 and –2.472 V, respectively. Absorption maxima for compounds **17–19** (Scheme 9) are similar to **15** and **16**, although the intensities of the absorptions are not quantified in the report [66]. Excited state energy levels of –2.67, –2.54 and –2.51 V for **17**, **18** and **19** have been estimated from absorption and electrochemical data. Sealed cells containing **15–19** as sensitizers were fabricated using a TiO_2/conductive glass photoanode and combined with a Pt-coated counter-electrode and I^-/I_3^-

electrolyte. Table 4 summarizes the DSC performance data for the cells illuminated under visible light (470 mW cm^{-2}). Once again, the low performance of the standard cells with N719 suggest that these data need to be treated with caution, and we note that the inclusion of mercury in dyes **17–19** must be regarded as a key negative aspect when considering the environmental acceptability and impact of these materials.

Table 3. Comparison of DSC performances using ferrocene-dyes functionalized with anchoring groups versus N719. The low performance of the standard N719 cell should be noted. Data from reference [64]; light intensity was 470 mW cm^{-2}.

Dye	V_{OC} / mV	J_{SC} / mA cm^{-2}	*ff*	η / %
	Propylene carbonate I^-/I_3^- electrolyte			
N719	790	12.72	0.66	1.4
12	648	8.28	0.71	0.81
13	660	7.24	0.67	0.68
14	640	7.60	0.71	0.73
	Ionic liquid I^-/I_3^- electrolyte			
12	640	7.96	0.63	0.66
13	650	6.89	0.62	0.58
14	630	7.26	0.66	0.64

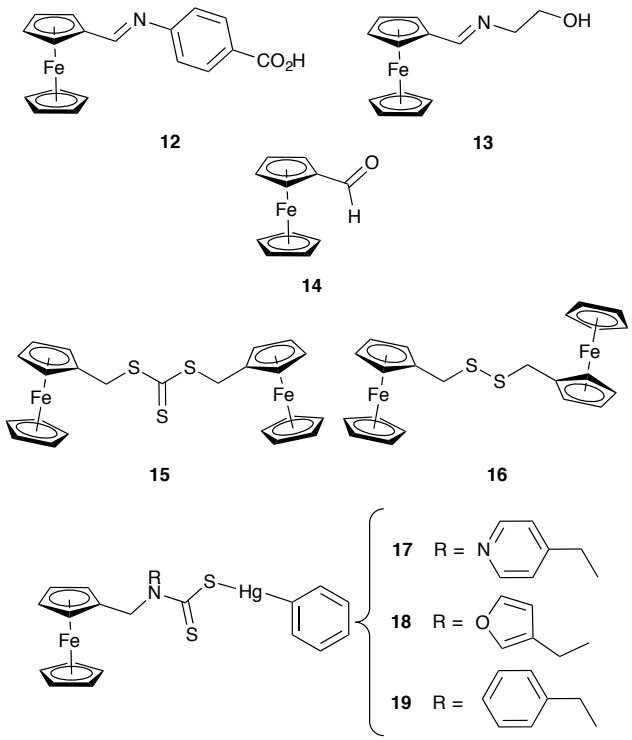

Scheme 9. Structures of ferrocene-derived compounds tested as sensitizers in DSCs.

Table 4. Performance data of DSCs containing the ferrocene-dyes **15–19** functionalized with anchoring groups versus N719. The low performance of the standard N719 cell should be noted. Data from references [65,66]; light intensity was 470 mW cm^{-2}.

Dye	V_{OC} / mV	J_{SC} / mA cm^{-2}	*ff*	η / %
	Data for dyes **15** and **16** relative to N719			
N719	761	8.72	0.71	1.00
15	647	8.38	0.72	0.83
16	641	7.04	0.71	0.68
	Data for dyes **17–19** relative to N719			
N719	750	8.95	0.70	1.0
17	630	7.88	0.65	0.71
18	630	7.32	0.64	0.65
19	630	7.02	0.63	0.62

Prussian blue-sensitized ZnO solar cells have been designed for use in economically deprived regions with the aim of producing small amounts of solar energy to harness for chlorination of drinking water. Although these solar cells are not the typical DSC design (Figure 3), we include them because of their simplicity and the fact that

components are chosen from readily available materials. Copper wire or carbonized wood coated with ZnO forms the working electrode, the latter being sensitized with Prussian blue. The photoelectrochemical cells were completed either with a copper counter-electrode and electrolyte comprising $CuSO_4$ and $FeSO_4$, or graphite counter-electrode and aqueous $[Fe(CN)_6]^{3-}/[Fe(CN)_6]^{4-}$ electrolyte. Table 5 shows open circuit voltage and short circuit current data for the solar cells and compares their performances with similarly constructed cells which used I^-/I_3^- electrolyte and Mercurochrome (Scheme 10) as sensitizer. The results demonstrate that it is possible to construct simple dye-sensitized photoelectrochemical cells that function with low efficiencies but without the need for expensive components [67,68]. The $[Fe(CN)_6]^{3-}/[Fe(CN)_6]^{4-}$ redox couple has also been studied as an electrolyte in conventional DSCs [69], its redox potential being close to that of the commonly employed I^-/I_3^- couple. Advantages of $[Fe(CN)_6]^{3-}/[Fe(CN)_6]^{4-}$ over I^-/I_3^- as an electrolyte include its less corrosive nature, and the fact that it can be employed in an aqueous medium although the toxicity is higher.

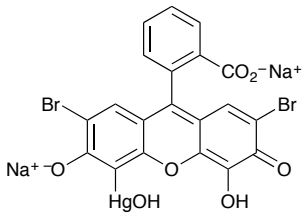

Scheme 10. The structure of Mercurochrome.

Table 5. Open circuit voltages and short circuit currents for simple solar cells with either Prussian blue or mercurochrome sensitizers. Data from reference [67].

Dye	Working electrode	Electrolyte	V_{OC} / mV	J_{SC} / mA cm^{-2}
Prussian blue	ZnO/carbonized wood	$[Fe(CN)_6]^{3-}/[Fe(CN)_6]^{4-}$	190-280	0.3-0.8
Prussian blue	ZnO/carbonized wood	I^-/I_3^-	620	0.5-1.0
Prussian blue	ZnO/copper	Cu^{2+}/Fe^{2+}	530	1.0-1.5
Mercurochrome	ZnO/carbonized wood	I^-/I_3^-	550-630	0.5-2.0
Mercurochrome	ZnO/TiO_2/ carbonized wood	I^-/I_3^-	630	1.0-2.0
Mercurochrome	ZnO/TiO_2/Cu	Cu^{2+}/Fe^{2+}	530	1.0-1.5

2.5 Cobalt

The importance of cobalt in DSCs primarily lies in its role as a redox mediator (i.e. the electrolyte). The I^-/I_3^- redox couple has been the workhorse of redox-shuttles since the conception of DSCs in the 1990s. However, disadvantages such as its reactivity, corrosive nature and the need to tune the redox couple to the Fermi level of new semiconductors and the energy levels of new dyes have led to significant efforts to find replacement electrolytes. Among the most encouraging alternatives are those based upon the Co^{2+}/Co^{3+} redox couple, for example, $[Co(tpy)_2]^{2+/3+}$, $[Co(bpy)_3]^{2+/3+}$, $[Co(phen)_3]^{2+/3+}$, $[Co(dmbip)_2]^{2+/3+}$ and $[Co(dbbip)_2]^{2+/3+}$ (dmbip and dbbip, see Scheme 11) [70]. In 2012, Hamann published a review [71], the title of which: '*The end of iodide? Cobalt complex redox shuttles in DSSCs*' indicates the progress that has been made in applying cobalt(III)/(II) polypyridyl complexes (typically combined with an organic dye) [72] in dye-sensitized solar cells. A recent review from Stergiopoulos and Falaras [24] provides an excellent overview of cobalt, copper, and ferrocene-based redox mediators, emphasizing means by which energy losses from DSCs can be minimized. In the light of these excellent recent reviews, we will not elaborate further on redox mediators in this article.

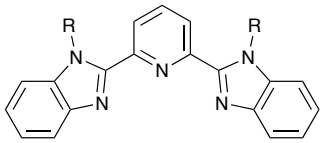

dmbip R = Me
dbbip R = ^{n}Bu

Scheme 11. Structures of 2,6-bis(1'-methylbenzimidazol-2'-yl)pyridine (dmbip) and 2,6-bis(1'-butylbenzimidazol-2'-yl)pyridine (dbbip).

2.6 Nickel

To date, the most common application of nickel in DSCs has been in the use of semiconducting NiO in photocathodes, typically in tandem cells [73], but a few nickel complexes have been used as photosensitizers in DSCs. Examples of nickel-based dyes include the dithiolene complexes in Scheme 12. Robertson and coworkers have reported complexes **20** with carboxylic acid or ester anchoring units. The molecules exhibit intense absorptions in the UV region and both complexes absorb in the visible region at 530 and 560 nm; for R = CO_2Et (Scheme 12), these bands have ε_{max} = 7300 $dm^3\ mol^{-1}\ cm^{-1}$. The performances of sealed DSCs employing **20** with R = CO_2H as

photosensitizer supported on an FTO/TiO_2 photoanode, Pt counter-electrode and I^-/I_3^- electrolyte were investigated. Different concentrations of cheno (**7**, Scheme 5) were added to some DSCs to counter the effects of aggregation of dye molecules through π-stacking; the effect of $TiCl_4$ post-treatment was also examined. The efficiencies of all the DSCs were low; η = 0.006–0.084% with respect to η = 3.000% for cells using the Pt(II) analog as photosensitizer; values of I_{SC} ranged from 0.090 to 0.293 mA and V_{OC} from 389 to 521 mV [74]. The near infrared (NIR) dyes **21** (Scheme 12) absorb with maxima in the 850-950 nm region and gave DSCs with efficiencies in the range 0.07-0.11% [75]. The related complexes **22** (Scheme 12) have also been reported. Electropolymerization of **22** produces films that exhibit the NIR light-harvesting properties of the parent molecules, and the rheological properties of the butyl chains result in high-quality spin-coated films [76,77]. The nickel(II) porphyrinato complex shown in Scheme 3a performs poorly as a sensitizer and exhibits an efficiency of only 0.05% compared to 5.85% for standard dye N3 (Scheme 1) measured under the same conditions; the zinc(II) analog is a more encouraging choice of dye (η = 8.60%) [32].

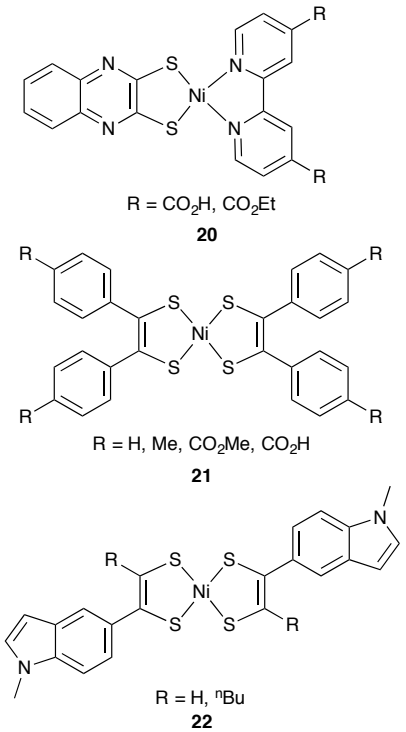

Scheme 12. Structures of nickel dithiolene sensitizers.

A nickel(II) coordination polymer (Scheme 13) containing a polycarbazole backbone and 8-hydroxyquinolinato metal-binding domains has been tested as a

photosensitizer in DSCs along with its zinc(II) analog. The TiO_2 electrode was soaked in a DMF solution of the Ni or Zn-containing sensitizer before combining with I^-/I_3^- electrolyte and platinized FTO counter-electrode. An efficiency of 0.45% was achieved for the nickel(II)-based sensitizer (J_{SC} = 1.27 mA cm^{-2}, V_{OC} = 650 mV, *ff* = 0.550) compared to 1.11% for the zinc(II)-based dye (J_{SC} = 2.52 mA cm^{-2}, V_{OC} = 745 mV, *ff* = 0.586) [78]. Related work centers on the copolymer dyes shown in Scheme 14 [79]. The electrochemical band-gaps of the Ni, Zn and Cd series of dyes are 2.24 eV (Ni), 2.18 eV (Zn) and 2.15 eV (Cd). Each DSC was fabricated using a dye-sensitized TiO_2 working electrode, a Pt counter electrode and I^-/I_3^- electrolyte. Values of V_{OC} for the three dyes are similar (580 mV for Ni, 590 mV for Zn, and 550 mV for Cd), while the J_{SC} values vary from 0.805 mA cm^{-2} for Ni, to 1.088 and 1.45 mA cm^{-2} for Zn and Cd. Fill factors for the Ni- and Cd-containing dyes are lower (0.593 and 0.55, respectively) than that for the Zn-based dye (0.648). Values of η range from 0.29% for the Ni-based dye to 0.44% for that containing Cd. The low J_{SC} for the Ni-based system is attributed to weak physisorption on the semiconductor, low charge separation and poor ability to transport holes to the electrolyte. Members of the second series of polymeric dyes (Scheme 14) contain thiophene–fluorene or thiophene–phenylene backbones which act as electron donors, and cobalt(II) or nickel(II) coordination domains functioning as electron acceptors. Open cells were fabricated with a FTO/TiO_2/dye working electrode, I^-/I_3^- electrolyte and Pt counter electrode. With incident light of intensity 100 mW cm^{-2}, the cells gave open-circuit voltages in the range 615–695 V, but very low values of J_{SC} (2.324 to 2.490 mA cm^{-2}) leading to low conversion efficiencies (0.96–1.21%). The poor J_{SC} values are attributed to a combination of poor dye adsorption, charge separation and low transport efficiency [80].

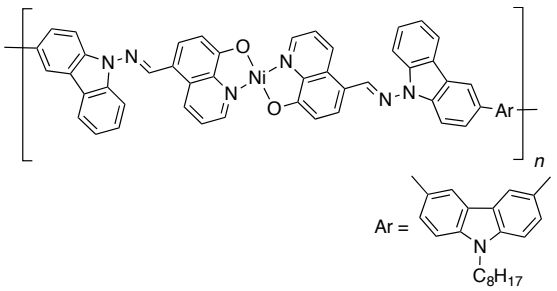

Scheme 13. Structure of a nickel(II) coordination polymer tested as a photosensitizer in a DSC; the zinc(II) analog has also been investigated.

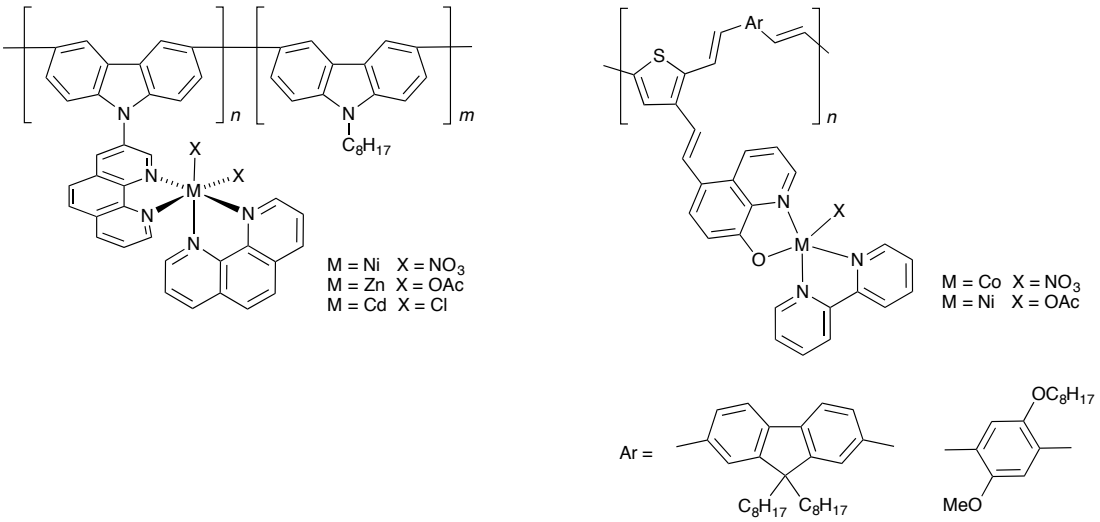

Scheme 14. Polymers carrying side-chain metal complexes tested as photosensitizers in DSCs.

A dye prepared from nickel(II) and the tetrasodium salt of **23** (Scheme 15) has been incorporated into a sealed DSC fabricated with a ZnO photoanode, platinized FTO counter-electrode and I^-/I_3^- electrolyte. The device performance is not promising (J_{SC} = 1.68 mA cm^{-2}, V_{OC} = 506 mV, *ff* = 0.41 when illuminated with a full spectrum); a maximum IPCE value of 8.7% (λ_{max} = 563 nm) was achieved [81].

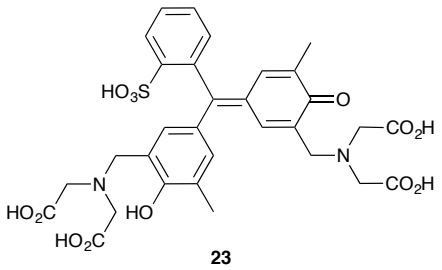

23

Scheme 15. The nickel(II) complex of the conjugate base of **23** has been tested as a sensitizer.

2.7 Copper

The application of copper in dyes in DSCs was highlighted by Robertson in 2008 [82] and copper is currently a front-runner for sensitizers among Earth abundant metals. Copper(I) complexes were first introduced into DSCs as sensitizers by Sauvage and co-workers [83] based on their similar photophysical properties to ruthenium(II) complexes [84,85]. The first study was made in photoelectrochemical cells based on thin film TiO_2 (anatase) and ZnO ceramic electrodes sensitized with complex **24**

(Scheme 16) bearing terminal carboxylate groups. Methanol solutions of **24** show a broad absorption in the visible region (λ_{max} = 440 nm, ε_{max} = 3000 dm^3 mol^{-1} cm^{-1}). The color intensity of **24** adsorbed on a surface is very dependent on the concentration of the initial solution, and the quantum efficiency depends on the degree of surface coverage of the complex. In a solar-cell configuration with a TiO_2 thin film electrode, I^-/I_3^- electrolyte and illumination via a bandpass filter (500 nm), V_{OC} was 600 mV with $J_{SC} \approx 0.6$ mA cm^{-2}. Since these first results, the use of copper(I) dyes has developed significantly and the use of DFT and TD-DFT calculations is proving to be of significant value in assisting in the design of copper(I)-containing sensitizers. A general conclusion from the work of Lu et al. is that the oligopyridine copper(I)-based complexes are suited as sensitizers. This group has investigated the molecular and electronic structures and electronic absorption spectra of the homoleptic and heteroleptic $\{Cu^I(bpy)_2\}$-based complexes shown in Scheme 17, both in the gas phase and MeCN solution, and with and without PF_6^- counter-ion [86,87]. The structure of a copper(I) bis(2,2'-biquinoline)-based complex (Scheme 17) has also been investigated at the TD-DFT level [88]. The pendant phenyl substituents in $[Cu(dpp)_2]^+$ (dpp = 2,9-diphenyl-1,10-phenanthroline), a complex related to **24**, protect the copper(I) center and also cause the coordination environment to be flattened rather than more regular tetrahedral; this leads to the MLCT state lifetime being independent of solvent in contrast to that of $[Cu(dmp)_2]^+$ (dmp = 2,9-dimethyl-1,10-phenanthroline). A combination of DFT and X-ray transient absorption spectroscopy has been used to better understand the properties of the photoexcited states of the complexes. A pertinent finding is that a change in ligand conformation involving twisting of the phenyl rings occurs upon excitation of $[Cu(dpp)_2]^+$ but this does not result in significant conjugation of the 1,10-phenanthroline and phenyl rings. Thus, the additional charge arising from formal oxidation of the metal center remains localized on the phen domains [89].

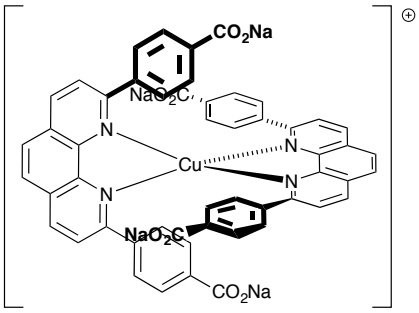

24

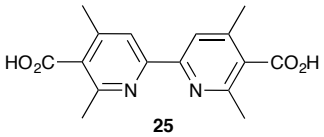

25

Scheme 16. The first copper(I) complex (**24**) investigated as a sensitizer in DSCs and an example of a bpy-based ligand (**25**) used in a homoleptic copper(I) dye.

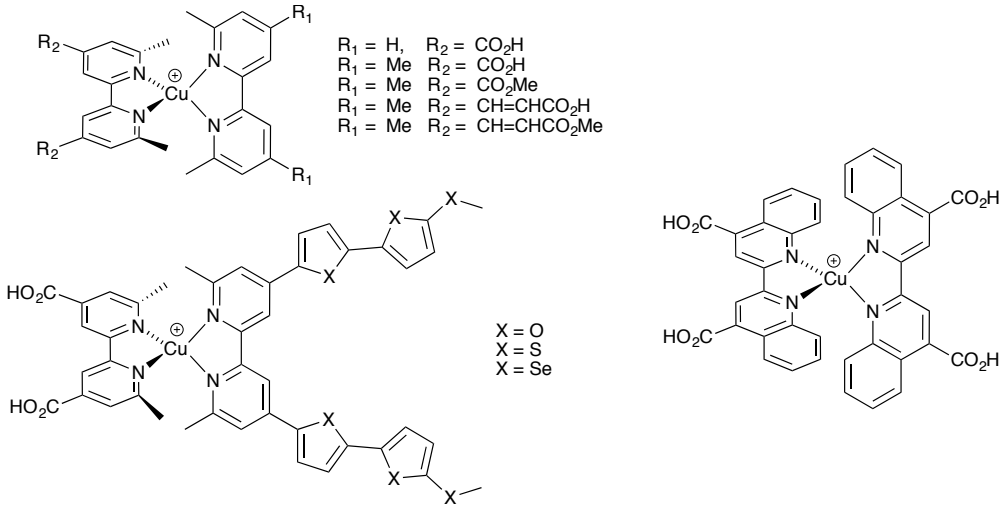

Scheme 17. Structures of some complexes studied computationally.

Sakaki and coworkers [90] have reported DSCs using the copper(I)-based sensitizer $[Cu(\mathbf{25})_2]^+$ (Scheme 16 shows ligand **25**). The complex exhibits a broad MLCT band around 450 nm (ε_{max} = 6400 dm^3 mol^{-1} cm^{-1} in MeOH). The maximum IPCE was 30% ($\lambda \approx$ 450 nm) under visible light irradiation of 100 mW cm^{-2}. The best DSC efficiency of 2.5% (J_{SC} = 4 mA cm^{-2}, V_{OC} = 630 mV) was obtained after optimization of TiO_2 sintering (500 ^{o}C for 30 min) and with I^-/I_3^- electrolyte. A long term stability test over 15 days showed a drop in V_{OC} to ≈500 mV within 24 h with little further decrease, while the photocurrent was maintained over the 15 day period.

Our own contributions to the area of DSCs containing copper(I) dyes have developed over the last five years, and have led us to establish a new protocol for *in*

situ dye assembly. We initially prepared a series of homoleptic copper(I) complexes of the 4,4'-disubstituted 6,6'-dimethyl-2,2'-bipyridines **26**–**29** (Scheme 18) [91]. Dyes $[Cu(\mathbf{26})_2]^+$ and $[Cu(\mathbf{28})_2]^+$ bind strongly to TiO_2, whereas $[Cu(\mathbf{29})_2]^+$ with the ester-anchors did not adsorb; the observation that $[Cu(\mathbf{27})_2]^+$ binds to TiO_2 can be rationalized in terms of ester hydrolysis and binding through carboxylic acid anchoring groups. Sealed DSCs fabricated using FTO/TiO_2 working electrodes, $[Cu(\mathbf{26})_2]^+$ or $[Cu(\mathbf{28})_2]^+$ dyes and I^-/I_3^- electrolyte were tested, and IPCE spectra and current-voltage characteristics for cells with $[Cu(\mathbf{26})_2]^+$ and $[Cu(\mathbf{28})_2]^+$ were significantly different. The extended π-conjugation in **28** leads to a higher molar extinction coefficient, and the DSC incorporating $[Cu(\mathbf{28})_2]^+$ exhibited an IPCE ($\lambda \approx 475$ nm) of 50% (compared to 38% of the DSC with $[Cu(\mathbf{26})_2]^+$). The device performances (Table 6) reveal unexpectedly high efficiencies of the carboxylic acid anchored copper(I) dyes. Investigation of solvent effects on dye deposition showed that EtOH is preferable to MeCN or ^{t}BuOH. Addition of cheno (**7**, Scheme 5) to decrease dye loading and improve the photovoltage unfortunately did not enhance the efficiency compared to a cell without cheno. Subsequently, we prepared complexes with 6,6'-disubstituted-2,2'-bipyridine ligands bearing anchoring groups in the 4,4' or 5,5'-positions (**30**–**33**, Scheme 18) [92]. Measurements were made with open cells, FTO/TiO_2 photoanodes, FTO/Pt counter-electrodes, I^-/I_3^- electrolyte and with a light intensity of 100 mW cm^{-2}. Due to a non-optimized cell construction, the efficiencies of the DSCs were lower than in our previous work. The complexes bind strongly to the TiO_2 layer giving a strongly red-colored surface, and the highest efficiencies were obtained for $[Cu(\mathbf{30})_2]^+$ and $[Cu(\mathbf{32})_2]^+$ (Table 7). The lower performance of the DSCs constructed with $[Cu(\mathbf{33})_2]^+$ versus $[Cu(\mathbf{32})_2]^+$ is rationalized in terms of a combination of the lower absorptivity of the complex and lower adsorption on TiO_2; the steric effects of the phenyl substituents probably contribute to this. Interestingly, even the dye bearing furan functionalities colored the TiO_2 layer indicating chemisorption of the dye.

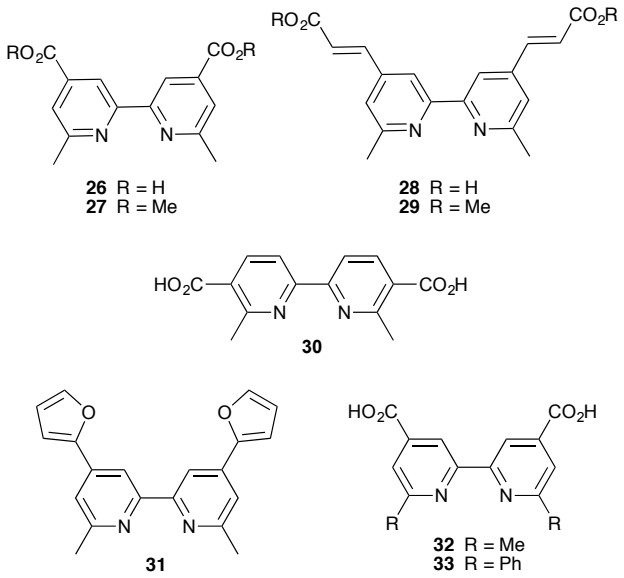

Scheme 18. Some 6,6'-disubstituted-2,2'-bipyridines used in copper(I) sensitizers.

Table 6. Performances of DSCs with two copper(I) dyes compared to N719. Data from reference [91].

Dye	V_{OC} / mV	J_{SC} / mA cm^{-2}	*ff*	η / %
[Cu(**26**)$_2$]$^+$	566	5.25	0.64	1.9
[Cu(**28**)$_2$]$^+$	556	5.9	0.7	2.3
N719	767	17.7	0.71	9.7

Table 7. Performances of DSCs with bpy-based copper(I) dyes compared to N719. Data from reference [92].

Dye (solvent)	V_{OC} / mV	J_{SC} / mA cm^{-2}	*ff*	η / %
[Cu(**30**)$_2$]Cl (MeOH)	570	1.21	0.65	0.45
[Cu(**32**)$_2$]Cl (MeOH)	530	1.15	0.68	0.41
[Cu(**33**)$_2$]Cl (DMSO)	484	0.69	0.63	0.21
[Cu(**31**)$_2$][PF_6] ($CHCl_3$)	490	0.46	0.62	0.14
N719 (MeCN)	750	11.3	0.67	5.0

A significant advance has been to utilize the lability of copper(I) diimine complexes to develop *in situ* stepwise assembly of the copper(I)-based sensitizer in a DSC. The method involves the initial binding of an anchoring ligand L_{anchor} to the semiconductor surface, followed by ligand exchange with a homoleptic $[CuL_2]^+$ complex (Scheme 19). Uptake of dye is evidenced by a change in the semiconductor surface from colorless to orange-red, the latter color arising from the adsorbed heteroleptic $[Cu(L_{anchor})(L)]^+$ complex. The rapid L_{anchor}/L ligand exchange at a labile

metal center such as copper(I) (d^{10}) cannot be achieved with kinetically inert ruthenium(II) centers (low-spin d^6) and this is the genesis of a powerful new method for the preparation of cells which have the potential for regeneration. This method also allows screening of relatively large numbers of dyes without the need for isolation of the heteroleptic copper(I) complexes. The latter is often not possible because of the rapid establishment of solution equilibria between statistical mixtures of homo- and heteroleptic species [93].

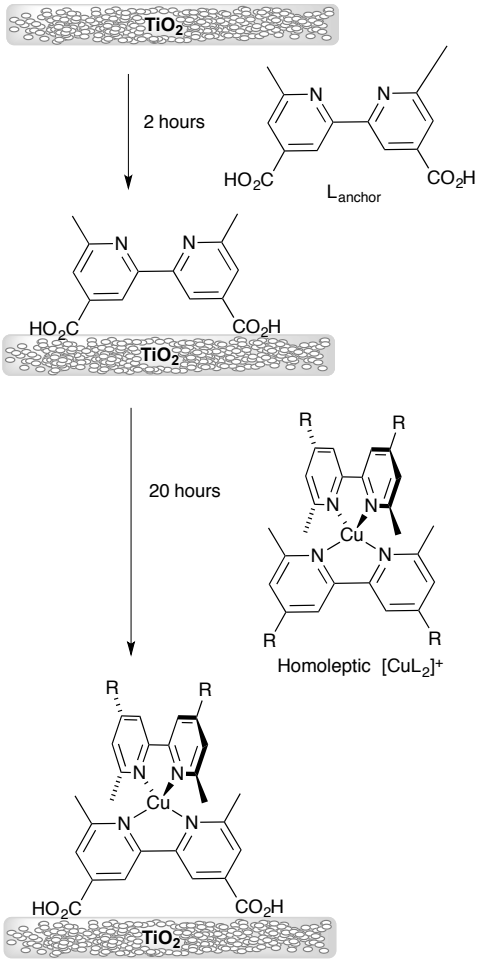

Scheme 19. The stepwise synthesis of a heteroleptic copper(I) complex in a DSC using an example of a typical anchoring ligand.

We have also prepared a series copper(I) complexes incorporating *N*-phenylpyridin-2-ylmethanimine. Here, the ligand design allows a homoleptic copper(I) complex to bind to TiO_2 through two carboxylate anchoring groups from two different ligands (Scheme 20). Open cell DSCs were constructed using an FTO/TiO_2/dye working electrode, FTO/Pt counter-electrode and I^-/I_3^- electrolyte, with measurements under

an irradiation of 100 mW cm^{-2}. Both $[Cu(\mathbf{34})_2]^+$ and $[Cu(\mathbf{34})(NCMe)_2]^+$ (see Scheme 20 for **34**) show relatively high surface coverage on TiO_2 (270 and 185 nmol cm^{-2}, respectively), but the efficiencies are <0.1%. The change from two anchoring groups to one on going from $[Cu(\mathbf{34})_2]^+$ to $[Cu(\mathbf{34})(NCMe)_2]^+$ does not decrease the power conversion efficiency. Although the surface coverage of 400 nmol cm^{-2} for $[Cu(\mathbf{35})_2]^+$ (see Scheme 20 for **35**) is encouraging, the overall efficiency of 0.23% (compared to 4.6% for standard dye N719 under the same conditions) is very low [94] and we have not pursued this ligand design strategy further. We note that the efficiency of 4.6% for N719 is relatively low; as our publications over the period 2009–2012 illustrate, changes to cell fabrication and improved semiconductor preparation result in a significant increase in this efficiency (to 9.90% [95]).

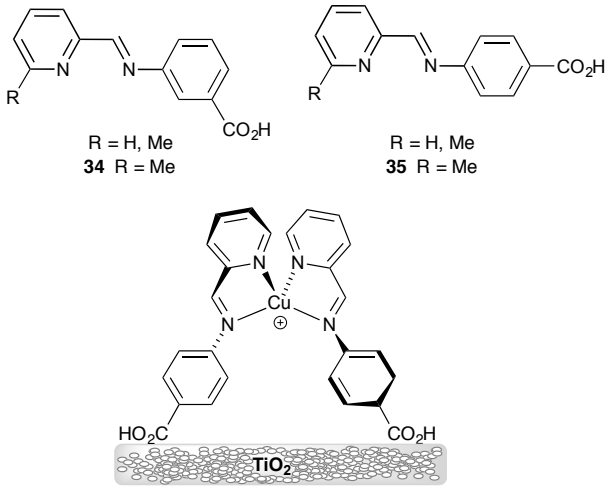

Scheme 20. A series of *N*-phenylpyridin-2-ylmethanimine ligands decorated with carboxylic acid anchoring groups and proposed binding mode to TiO_2.

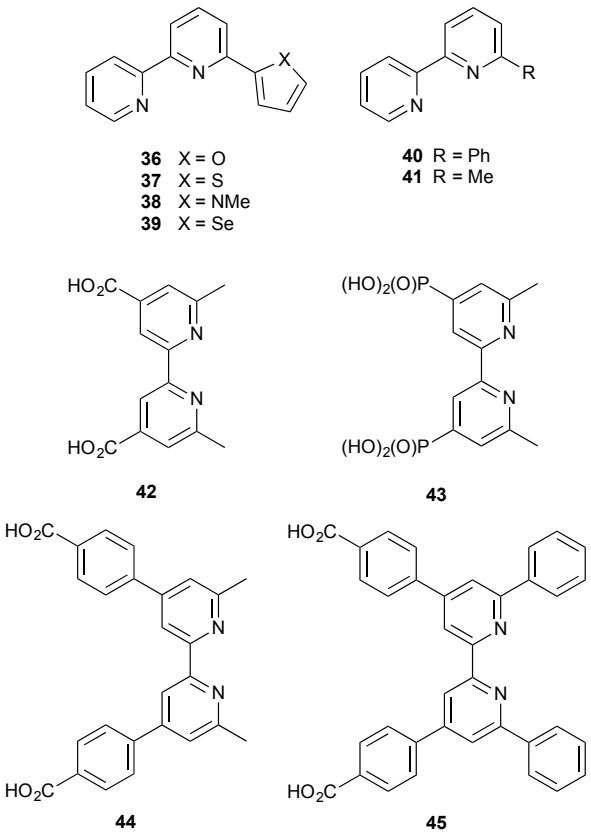

Scheme 21. Ancillary 6-functionalized 2,2'-bipyridines (**36–41**) and 6,6'-dimethyl- or 6,6'-diphenyl-2,2'-bipyridine-based anchoring ligands (**42–45**) used in heteroleptic copper(I) dyes.

Applying the above methodology for the stepwise assembly of surface-bound heteroleptic copper(I) complexes, we have screened a series of DSCs using ligand exchange reactions between the homoleptic complexes $[CuL_2][PF_6]$ (L = **36–41**, Scheme 21) and the surface-bound anchoring ligands **42**–**45** (Scheme 21) to produce 24 surface-anchored heteroleptic $[Cu(L_{anchor})(L)]^+$ complexes. Evidence for the formation of heteroleptic species on TiO_2 was obtained by using MALDI-TOF mass spectrometry and solid-state diffuse reflectance absorption spectroscopy. The DSCs were constructed using FTO/TiO_2/dye photoanodes, FTO/Pt counter-electrodes and I^-/I_3^- electrolyte and were measured under irradiation of 100 mW cm^{-2}. The highest efficiencies (1.20 to 1.51% compared to 4.50% for N719 under the same conditions) were observed with anchoring ligand **43** which binds through phosphonate groups [96]. This is a recurring feature, pointing to phosphonate anchors being particularly advantageous. To further improve copper(I)-based DSC performance, the homoleptic

copper(I) complex $[Cu(\mathbf{46})_2]^+$ has been designed (ligand **46** is shown in Scheme 22). The model compound $[Cu(\mathbf{47})_2][PF_6]$ (**47** = 6,6'-dimethyl-2,2'-bipyridine, Scheme 22) is red with an MLCT band at 452 nm, whereas the orange color of $[Cu(\mathbf{46})_2][PF_6]$ is consistent with the tail into the visible region of an intense absorption with λ_{max} = 400 nm. Both $[Cu(\mathbf{46})_2]^+$ and $[Cu(\mathbf{47})_2]^+$ are redox active; however, while $[Cu(\mathbf{47})_2][PF_6]$ exhibits both copper- and ligand-based processes, the behaviour of $[Cu(\mathbf{46})_2][PF_6]$ is dominated by ligand-based processes. Using our surface ligand-exchange methodology, eight TiO_2 surface-bound heteroleptic complexes incorporating anchoring ligands **42**–**45** and ancillary ligands **46** and **47** were prepared. The presence of the extended π-system in **46** significantly improves dye performance, and the most efficient sensitizers are those using anchoring ligands **43** and **44**. A combination of $[Cu(\mathbf{46})_2]^+$ with the phosphonate anchor **43** gives a very promising performance (η = 2.35% compared to 7.29% for N719); sealed cells were made using FTO/TiO_2/dye photoanodes, FTO/Pt counter-electrodes and I^-/I_3^- electrolyte. The DSC efficiency was either similar or enhanced over 2 or 5 days after sealing of the cells. TD-DFT calculations were used to predict the electronic absorption spectra of the heteroleptic complexes $[Cu(\mathbf{46})(L_{anchor})]^+$ and $[Cu(\mathbf{47})(L_{anchor})]^+$ (L_{anchor} = **42**, **43**, **44**) and the transitions making up the dominant bands were analysed in terms of the character of the HOMO–LUMO orbital manifold. For $[Cu(\mathbf{47})(\mathbf{43})]^+$ and $[Cu(\mathbf{47})(\mathbf{44})]^+$, metal-to-anchoring ligand transitions contribute considerably to the absorptions. In contrast, for $[Cu(\mathbf{47})(\mathbf{42})]^+$, character from the anchoring ligand **42** is hardly involved. This is consistent with the poor device performance of $[Cu(\mathbf{47})(\mathbf{42})]^+$. For $[Cu(\mathbf{46})(\mathbf{43})]^+$, calculations show dominant anchoring ligand character in the LUMO as is required for efficient electron injection; in practice, $[Cu(\mathbf{46})(\mathbf{43})]^+$ is the most efficient dye of the eight screened. The orbital composition of the HOMOs of the two most efficient dyes ($[Cu(\mathbf{46})(\mathbf{43})]^+$ and $[Cu(\mathbf{46})(\mathbf{44})]^+$) is dominated by character from ancillary ligand **46**, suggesting that the presence of **46** improves the performance of the dye by minimizing back-migration of an electron from the semiconductor to the sensitizer [97].

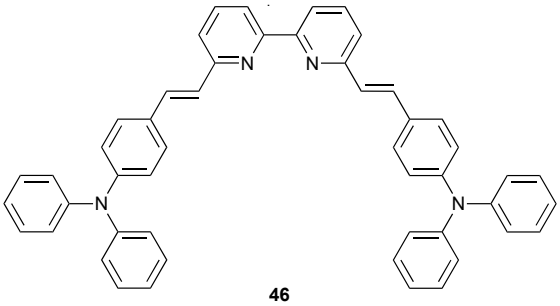

46

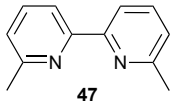

47

Scheme 22. Ancillary ligand **46** which exhibits extended π–conjugation and model ligand **47**.

Recently, we have turned our attention to the incorporation of hole-transport triphenylamino-dendrons into the ancillary ligands (Scheme 23) in heteroleptic copper(I) DSCs and have shown that this strategy greatly enhances the performance of the dyes. Sealed cells were assembled (FTO/TiO_2/dye photoanodes, FTO/Pt counter-electrodes, I^-/I_3^- electrolyte) using ligand exchange between homoleptic copper(I) complexes of the first and second-generation ligands shown in Scheme 23 on a TiO_2 surface functionalized with anchoring ligands **42**, **43** and **44** (Scheme 21). The device characteristics reveal that extending the dendron from first to second generation results in an increase in J_{SC} as well as, in most cases, an increase in V_{OC}; the improvement in short circuit current density is more significant than that in open-circuit voltage. The most efficient dye reached η = 2.37% compared to 9.90% for N719 is **48** (Scheme 23) and its internal quantum efficiency (IQE)[a] spectrum closely resembles the absorption spectrum of the homoleptic complex in the visible region (λ = 460 nm , IQE = 27%) [95]. As mentioned in Section 1.2, best practice is for the use of masked DSCs [28], and we have now introduced this routinely in our work. Complete masking of cells ensures that short circuit current densities are not over-estimated, and of course results in lower power conversion efficiencies than for the corresponding cell when it is unmasked. Significantly, however, we have shown that

[a] IQE is related to EQE by the equation: $IQE = \frac{EQE}{(1-T-R)}$ where T and R are the transmission and reflection of incoming light.

the relative efficiencies of series of dyes with respect to N719 are similar whether the cells are unmasked or masked [95].

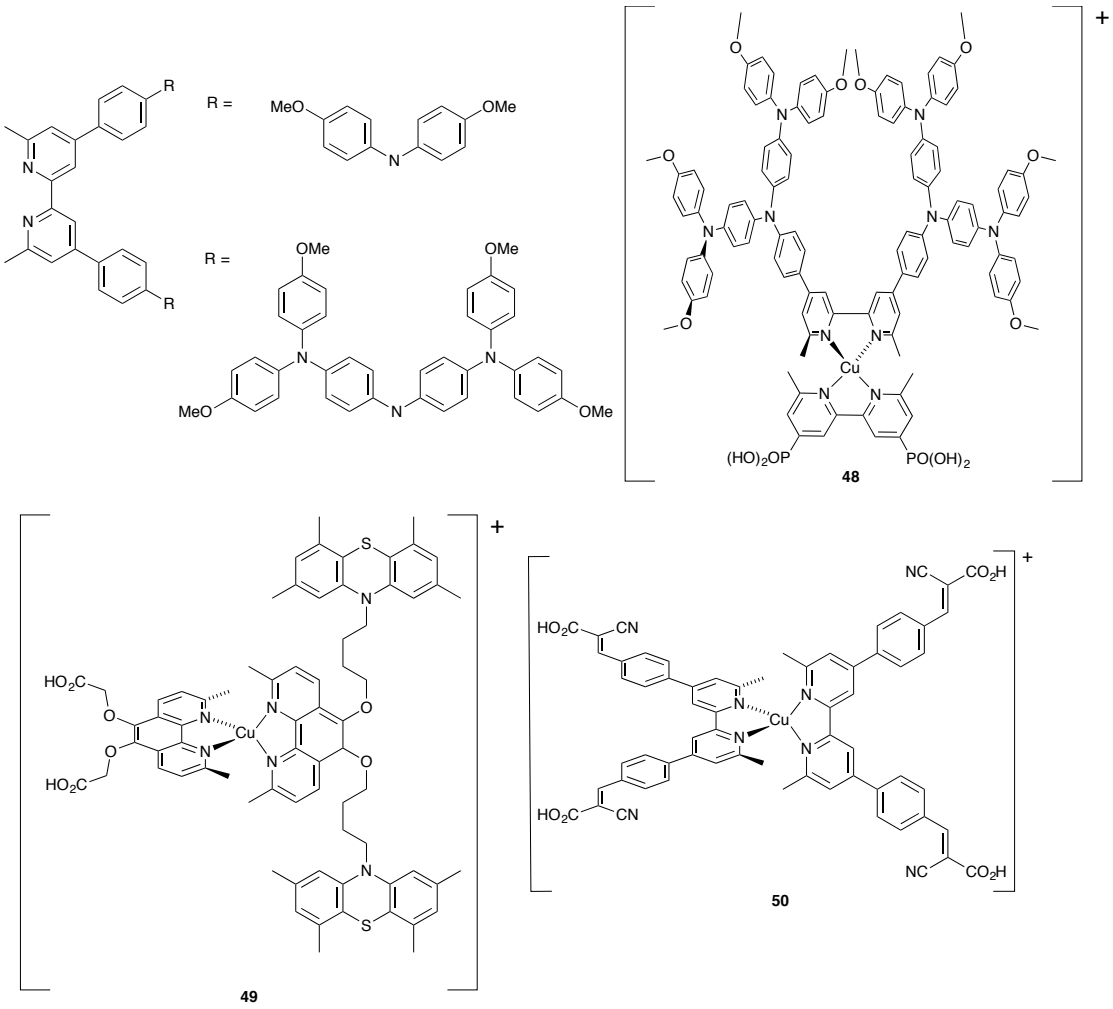

Scheme 23. Ligands incorporating first- and second generation hole-transporting dendrons, and the structures of three efficient copper(I) sensitizers, **48–50**.

Many of the design features in dyes are illustrated in studies of **49** and related species which have been prepared using the surface assembly methodology. The peripheral ligand incorporates a phenothiazine, which rapidly delivers an electron to the copper(II) center generated after injection to facilitate the electron-hole separation and reduce the rate of the back-reaction [98]. Copper(I) dye **50** (Scheme 23) exhibits good properties as a sensitizer in DSCs [99]. The absorption spectrum of a MeOH solution of **50** shows an intense ligand-based $\pi^* \leftarrow \pi$ band at 310 nm ($\varepsilon = 5.54 \times 10^4$ dm^3 mol^{-1} cm^{-1}) and an MLCT band at 496 nm (ε = 8033 dm^3 mol^{-1} cm^{-1}). Unfortunately, the excited-state lifetime of the complex is very short. The authors note the problems associated with the less rigid 2,2-bipyridine scaffold compared to

that of the 1,10-phenanthroline metal-binding domain [100]. DFT calculations on **50** reveal that the HOMO is predominantly copper-based, while the LUMO possesses character from the bpy and anchoring units, a prerequisite for efficient electron injection from the excited state. Open-cell DSCs were made using an FTO/TiO_2/dye working electrode, I^-/I_3^- electrolyte and Pt counter-electrode and illumination for the measurements was 100 mW cm^{-2}. Device characteristics were V_{OC} = 570 mV, J_{SC} = 4.69 mA cm^{-2} and *ff* = 0.788, and a relatively high power conversion efficiency of 2.2% compared to η = 7.8% for N719 was observed.

The complex [Cu(**51**)(**52**)]$^+$ illustrates the effects of combining N^N and P^P donor sets (Scheme 24) in a copper(I) dye. The ancillary ligand **52** is bulky and geometrically inflexible, allowing a bpy-derived anchoring ligand without 6,6'-substituents (**51**) to be used. Acetonitrile solutions of [Cu(**51**)(**52**)][BF_4] exhibit a strong absorption (π∗←π) at 276 nm and a weaker MLCT band at 416 nm. UV-VIS absorption spectra predicted from TD-DFT calculations agree well with the experimental data. DSCs were prepared as sealed cells with [Cu(**51**)(**52**)]$^+$ as sensitizer and I^-/I_3^- electrolyte and were measured under illumination of 100 mW cm^{-2}. The observed V_{OC} was consistently around 350 mV, and the inclusion of cheno (Scheme 5) in the dye baths improved I_{SC} by minimizing dye aggregation. The optimum ratio of dye : cheno was 1 : 1. The best efficiency was ≈0.05% compared to 3.05% for N719 [101]. Little work has been reported concerning heterometallic dyes containing copper. Spectroelectrochemical and EPR data coupled with TD-DFT computational results indicate that the first oxidation potential of complex **53** (Scheme 24) is based mainly on ruthenium, but that there is little difference between the energies of Ru- and Cu-based HOMOs. Complex **53** absorbs strongly in the visible region (λ_{max} = 562 nm, ε_{max} = 22200 dm^3 mol^{-1} cm^{-1}), the maximum correlating well with the maximum IPCE of 31% at 545 nm. Sealed DSCs constructed using FTO/TiO_2/**53** photoanodes, I^-/I_3^- electrolyte and FTO/Pt counter electrodes produced an efficiency of 2.55% (compared to 6.4% for N719); V_{OC} = 608 mV, J_{SC} = 5.84 mA cm^{-2} and *ff* = 0.72. Under prolonged irradiation (AM1.5), the cells show an increased efficiency with time [102].

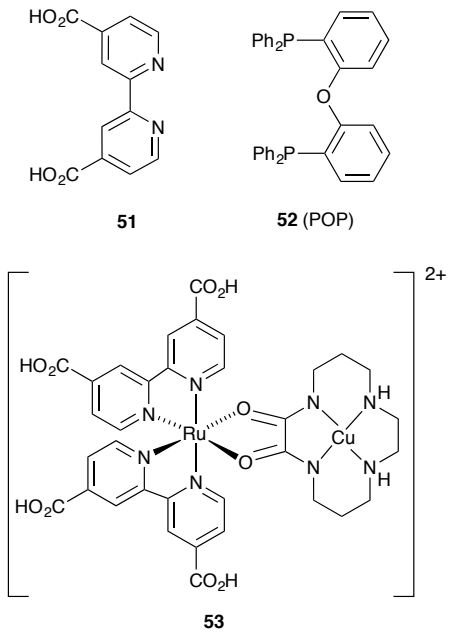

Scheme 24. Structures of ligands **51** and **52** and the heterometallic complex **53**.

Copper complexes studied as sensitizers are typically 4-coordinate copper(I), with the copper(I) sterically protected to prevent a change to a square-planar geometry that accompanies oxidation to copper(II). In contrast, the dye $[Cu(bpy)_2(NO_3)]^+$ contains 5-coordinate copper(II) with the coordinated nitrato-ligand acting as the anchor on TiO_2. Presumably, electron injection to the photoanode is concomitant with ligand (not copper) oxidation. The reflectance UV/VIS spectrum of $[Cu(bpy)_2(NO_3)]^+$ exhibits bands at 245 and 280 nm (bpy-based transitions), 350-600 nm (MLCT) and a 650 nm (broad). Sealed DSCs were fabricated with FTO/TiO_2/dye working electrode, FTO/Pt counter-electrode and I^-/I_3^- electrolyte. However, only a very low conversion efficiency of 0.032% was achieved compared to 3.0–5.0% for N719, with a low open-circuit voltage (346 mV) and low values of J_{SC} = 0.166 mA cm^{-2} and *ff* = 0.55 (light intensity = 100 mW cm^{-2}) [103]. These results indicate that bis(bpy) copper(II) complexes have no advantage over copper(I) dyes.

2.8 Zinc

Zinc(II) porphyrinato complexes have been included in a recent review and will not be discussed further here [5]. Schemes 13 and 14 showed polymeric complexes incorporating Ni, Zn and Cd and the performances of these dyes in DSCs have already been discussed [78,79]. The thiophene-containing polymeric photosensitizers shown in Scheme 14 have been extended to polymers **54** and **55** (Scheme 25) [104].

Their absorption spectra show bands in the UV at 356, 337 and 323 nm, respectively, assigned to ligand-centered $\pi^* \leftarrow \pi$ transitions. Good thermal stabilities are exhibited by both complexes. Cell fabrication used a FTO/TiO_2 working electrode dipped into a DMSO solution of the dye, Pt foil counter-electrode and I^-/I_3^- electrolyte; illumination intensity was 100 mW cm^{-2}. Zhong and co-workers [105] have also prepared polymers **56** and **57** (Scheme 25, and compare with Scheme 14); these are thermally stable with 5% weight loss (under N_2) at 364 ^oC for M = Cd and 277 ^oC for M = Zn. The UV/VIS absorption spectra in DMF solution shows that **56** and **57** exhibit intramolecular charge-transfer bands at 434 and 451 nm, respectively, and MLCT bands 512 and 541 nm, respectively, and the electrochemical band-gaps are 2.393 and 2.303 eV for **56** and **57**. The complexes were used as sensitizers in DSCs constructed using a FTO/TiO_2/dye photoanode, Pt counter-electrode and I^-/I_3^- electrolyte (incident light intensity = 100 mW cm^{-2}). The performances of the devices with **54–57** are summarized in Table 8, but as no standard dye was used as a reference, it is difficult to assess the merits of these polymeric sensitizers.

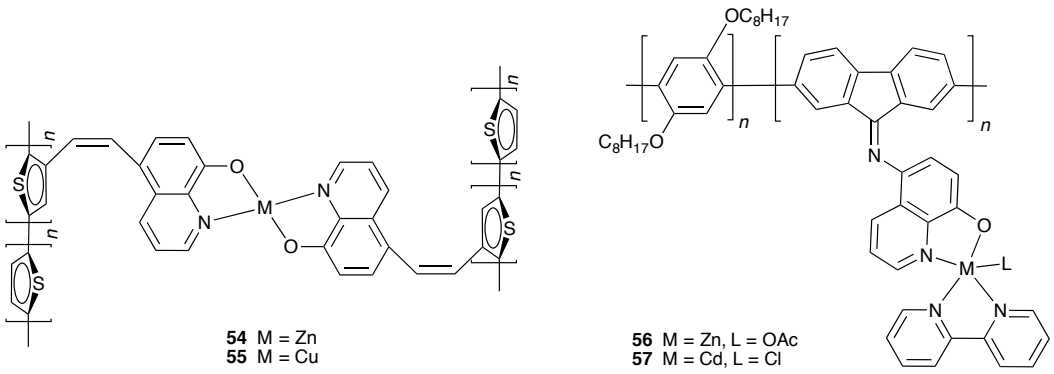

Scheme 25. Examples of polymeric photosensitizers containing zinc(II), copper(II) and cadmium(II). See also Schemes 13 and 14.

Table 8. Photovoltaic performances of DSCs with polymeric metal complexes as sensitizers. Data from references [104,105].

Dye	V_{OC} / mV	J_{SC} / mA cm^{-2}	*ff*	η / %
54	610	1.55	0.59	0.56
55	630	1.872	0.65	0.78
56	0.59	0.69	0.60	0.24
57	0.62	0.83	0.62	0.32

Our group has introduced a new strategy for zinc-based DSC fabrication. In terms

of Figure 4, the surface-supported dye consists of an anchoring domain (in this case, ligand **58**, **59** or **60**, Scheme 26), an ancillary ligand and the zinc(II) ion. Since zinc(II) does not absorb in the visible region, the choice of ancillary ligands is crucial for photon capture. We chose **61** and **62** (Scheme 26) for their extended π-conjugation and hole-transporting triphenylamine units. FTO/TiO_2 anodes were first functionalized with **58**, **59** or **60** by immersion in a DMSO solution of the ligand. After 24 hours, the functionalized surface was treated with zinc(II) acetate or chloride, and the assembly of the dye was completed by dipping the anode in a CH_2Cl_2 solution of **61** or **62** for 64 hours. A persistent orange coloration of the titanium dioxide implied complex formation on the surface, and this was confirmed by solid state absorption spectroscopy. The working electrode was combined with a FTO/Pt counter-electrode in a sealed cell with I^-/I_3^-electrolyte. Measurements were made under irradiation of 100 mW cm^{-2} and the device characteristics are given in Table 9; measurements were repeated 2 and 7 days after sealing of the DSCs and the results confirmed that the zinc(II) complexes are stable sensitizers [106]. The observed efficiencies of these relatively simple zinc(II) sensitizers are extremely promising, prompting us to actively pursue suitable adaptations to the ancillary tpy ligand to enhance light-harvesting.

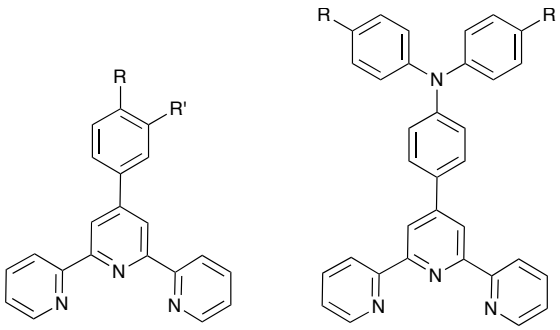

58 R = R' = CO_2H
59 R = R' = OH
60 R = $PO(OH)_2$ R' = H

61 R = H
62 R = OMe

Scheme 26. 2,2':6',2"-Terpyridines used as anchoring (**58–60**) and ancillary (**61**, **62**) ligands in zinc(II) sensitizers.

Table 9. DSCs efficiency data for zinc(II) dyes compared to standard dye N719 measured under the same conditions. Data from reference [106].

Zinc salt	L_{anchor}	Ancillary ligand	V_{OC} / mV	J_{SC} / mA cm^{-2}	*ff*	η / %
$Zn(OAc)_2$	**61**	**58**	538	0.002	0.52	0.59
$ZnCl_2$	**61**	**58**	546	0.003	0.52	0.71
$Zn(OAc)_2$	**62**	**58**	544	0.002	0.66	0.56
$ZnCl_2$	**62**	**58**	521	0.001	0.64	0.46
$Zn(OAc)_2$	**62**	**59**	529	0.001	0.68	0.41
$ZnCl_2$	**62**	**59**	521	0.001	0.54	0.34
$ZnCl_2$	**62**	**60**	536	0.002	0.61	0.55
N719			718	0.018	0.58	7.29

Sensitizers for DSCs based on the 5-coordinate zinc(II) complex **63** (Scheme 27) and its mercury and cadmium analogs have been reported. The conversion efficiency could be improved by using N719 as a co-sensitizer and ZnO photoelectrodes. The ZnO anodes were immersed in a solution of the dye followed by a solution of N719, and the DSCs were completed with FTO/Pt counter-electrodes and I^-/I_3^- electrolyte; power conversion efficiencies were measured under 100 mW cm^{-2} light intensity. The IPCE spectrum of the **63**/N719 DSC exhibited two maxima (35% at 400 nm and 30% at 530 nm). An overall solar-to-energy conversion efficiency of 3.378% for the zinc(II)-containing dye is notably higher than that achieved for N719 alone (1.909%), and it is proposed that the enhancement arises from a decrease in internal cell resistance in addition to improved UV-spectral response [107]. We note however, that the efficiency reported in this work for N719 is very low.

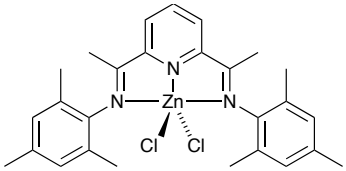

63

Scheme 27. Structure of the 5-coordinate zinc(II) complex **63**.

3 Overview and conclusions

This review has attempted to give a comprehensive survey of the use of first row transition metal complexes in photovoltaic cells. The final impression is one of

optimism that in the mid-term it may be possible to partially or completely replace materials based on platinum group metals by those involving Earth abundant metals. Our primary aim in writing this review was to pull together the disparate complexes of earth abundant metals employed as dyes in DSCs and to encourage further research in this area.

One point that has emerged in our collating the information for this review is the lack of consistency in the literature in presenting device data for DSCs. In particular, we urge authors to provide precise details of electrolytes and any additives that are used as well as the precise architecture of the TiO_2 nanoparticle phase including the number of layers and the deposition method as well as the presence or absence of compact or scattering layers. We strongly recommend that authors also report the performance of a standard dye such as N719 in their experimental system, using electrodes with identical characteristics to those in DSCs being screened. We found varying standards of reporting of cell fabrication and I–V data and, as with the recent publication from Snaith[28] that points to best practice for measuring solar cells, we consider that an important take-home message from this review is for consistency between measurements so that it becomes valid and meaningful to compare literature data from different sources.

Finally, we concur with most others who have attempted to review data relating to conventional DSCs that the irreproducibility of results makes claims of "the best" or "the most efficient" very difficult to evaluate. We fully agree with the calls for the use of certified measurements to establish such claims. In contrast, synthetically lead results in which new dye classes or new additives or electrolytes are evaluated are more often at the proof-of-concept stage and we recommend the use of comparative measurements with standard dyes under the authors' own experimental conditions.

4 Acknowledgements

We take this opportunity to thank all of the co-workers in our research group who have contributed to our own efforts in this exciting and emerging area of materials chemistry. ECC would like to acknowledge the European Research Council (Advanced Grant 267816 LiLo) which is providing partial support for our research activities in the area of sustainable materials chemistry.

References

[1] http://ec.europa.eu/energy/publications/doc/2012_energy_roadmap_2050_en.pdf.

[2] G. C. Vougioukalakis, A. I. Philippopoulos, T. Stergiopoulos, P. Falaras, Coord. Chem. Rev. 255 (2011) 2602 and references therein.

[3] Data from the US Geological Survey: http://minerals.usgs.gov/minerals/pubs/mcs/2012/mcs2012.pdf

[4] http://en.wikipedia.org/wiki/Abundance_of_the_chemical_elements

[5] L.-L. Li, E. W.-G. Diau, Chem. Soc. Rev. 42 (2013) 291.

[6] X. Li, H. Wang, H. Wu, Struct. Bond. 135 (2010) 229.

[7] M. G. Walter, A. B. Rudine, C. C. Wamser, J. Porphyr. Phthalocyan. 14 (2010) 759.

[8] J. N. Clifford, M. Planells, E. Palomares, J. Mater. Chem. 22 (2012) 24195.

[9] A. Mishra, M. K. R. Fischer, P. Bäuerle, Angew. Chem. Int. Ed. 48 (2009) 2474.

[10] L. Sun, L. Hammarström, B. Åkermark, S. Styring, Chem. Soc. Rev. 30 (2001) 36.

[11] L. Hammarström, L. Sun, B. Åkermark, S. Styring, Spectrochim. Acta, A 57 (2001) 2145.

[12] L. Hammarström, Curr. Opinion Chem. Biol. 7 (2003) 666.

[13] E. H. Arifin, W. R. Majlan, W. Daud, M. B. Kassin, Int. J. Hydrogen Energy 37 (2012) 3066.

[14] J. J. Concepcion, J. W. Jurss, M. K. Brennaman, P. G. Hoertz, A. O. T. Patrocinio, N. Y. M. Iha, J. L. Templeton, T. J. Meyer, Acc. Chem. Res. 42 (2009) 1954.

[15] C. J. Gagliardi, B. C. Westlake, C. A. Kent, J. J. Paul, J. M. Papanikolas, T. J. Meyer, Coord. Chem. Rev. 254 (2010) 2459.

[16] Md. K. Nazeeruddin, E. Baranoff, M. Graetzel, Solar Energy, 2011, 85, 1172.

[17] M. Grätzel, Acc. Chem. Res. 42 (2009) 1788.

[18] M. Grätzel, Inorg. Chem. 44 (2005) 6841.

[19] S. Anderson, E. C. Constable, M. P. Dare-Edwards, J. B. Goodenough, A. Hamnett, R. D. Wright, K. R. Seddon, Nature, 1979, 280, 571.

[20] M. Grätzel, Acc. Chem. Res., 2009, 42, 1788.

[21] S. Raga, E. M. Barea, F. Fabregat-Santiago, J. Phys. Chem. Lett. 3 (2012) 1629;

[22] J. Bisquert, ChemPhysChem 12 (2011) 1633.

[23] F. Sauvage, J.-D. Decoppet, M. Zhang, S. M. Zakeeruddin, P. Comte, M. Nazeeruddin, P. Wang, M. Grätzel, J. Am. Chem. Soc. 133 (2011) 9304.

[24] T. Stergiopoulos, P. Falaras, Adv. Energy Mater. 2 (2012) 616.

[25] G. C. Vougioukalakis, T. Stergiopoulos, A. G. Kontos, E. K. Pefkianakis, K. Papadopoulos, P. Falaras, Dalton Trans. 42 (2013) 6582 and references therein.

[26] A. Hagfeldt, G. Boschloo, L. Sun, L. Kloo, H. Pettersson, Chem. Rev. 110 (2010) 110, 6595.

[27] http://www.solaronix.com/documents/dye_solar_cells_for_real.pdf.

[28] H. J. Snaith, Energy Envir. Sci. 5 (2012) 6513.

[29] M. V. Martínez-Díaz, G. de la Torre, T. Torres, Chem Commun. 46 (2010) 7090.

[30] E. Palomares, M. V. Martínez-Díaz, S. A. Haque, T. Torres, J. R. Durrant, Chem. Commun. (2004) 2112.

[31] X. Zarate, E. Schott, R. Arratia-Pérez, Int. J. Quantum Chem. 111 (2011) 4186.

[32] C.-Y. Lin, C.-F. Lo, M.-H. Hsieh, S.-J. Hsu, H.-P. Lu, E. W.-G. Diau, J. Chin. Chem. Soc. 57 (2010), 1136.

[33] N. Xiang, W. Zhou, S. Jiang, L. Deng, Y. Liu, Z. Tan, B. Zhao, P. Shen, S. Tan, Solar Ener. Mater. Solar Cells 95 (2011) 1174.

[34] Y. Shen, F. Zheng, W. Cheng, F. Gu, J. Zhang, Y. Xia, Semicond. Sci. Technol. 25 (2010) 065016.

[35] F. Ambrosio, N. Martsinovich, A. Troisi, J. Phys. Chem. Lett. 3 (2012) 1531.

[36] W. R. McNamara, R. C. Snoeberger III, G. Li, C. Richter, L. J. Allen, R. L. Milot, C. A. Schmuttenmaer, R. H. Crabtree, G. W. Brudvig, V. S. Bastida, Energy Environ. Sci. 2 (2009) 1173.

[37] A. S. Polo, M. K. Itokazu, N. Y. M. Iha, Coord. Chem. Rev. 248 (2004) 1343.

[38] P. S. Johnson, P. L. Cook, I. Zegkinoglu, J. M. García-Lastra, A. Rubio, R. E. Ruther, R. J. Hamers, F. J. Himpsel, J. Chem. Phys. 138 (2013) 044709.

[39] S. Ferrere, B. A. Gregg, J. Am. Chem. Soc. 120 (1998) 843.

[40] A. L. Smeigh, J. K. McCusker, Springer Series in Chemical Physics, 88 (2007) pp 273-275.

[41] S. Ferrere, Chem. Mater. 12 (2000) 1083.

[42] S. Ferrere, Inorg. Chim. Acta 329 (2002) 79.

[43] A. A. Schilt, J. Am. Chem. Soc. 82 (1960) 3000.

[44] M. Yang, D. W. Thompson, G. J. Meyer, Inorg. Chem. 39 (2000) 3738.

[45] M. Yang, D. W. Thompson, G. J. Meyer, Inorg. Chem. 41 (2002) 1254.

[46] E. Vrachnou, N. Vlachopoulos, M. Grätzel, J. Chem. Soc., Chem. Commun., (1987) 868.

[47] E. Vrachnou, M. Grätzel, A. J. J. McEvoy, Electroanal. Chem. 258 (1989) 193.

[48] F. De Angelis, A. Tilocca, A. Selloni, J. Am. Chem. Soc. 126 (2004) 15024.

[49] J. E. Monat , J. K. McCusker, J. Am. Chem. Soc. 122 (2000) 4092.

[50] S.-H. Hwang, C. N. Moorefield, P. Wang, F. R. Fronczek, B. H. Courtney, G. R. Newkome, Dalton Trans. (2006) 3518.

[51] D. N. Bowman, E. Jakubikova, Inorg. Chem. 51 (2012) 6011.

[52] X. Lu, S. Wei, C.-M. L. Wu, N. Ding, S. Li, L. Zhao and W. Guo, Int. J. Photoenergy (2011) article 316952.

[53] A. Govindasamy, C. Lv, H. Tsuboi, M. Koyama, A. Endou, H. Takaba, K. Hiromitsu. M. Kubo, C. A. Del Carpio, A. Miyamoto, Akira, Jap. J. Appl. Phys. 46 (2007) 2655.

[54] P. V. Bernhardt, G. K. Boschloo, F. Bozoglian, A. Hagfeldt, M. Martınez, B. Sienra, New. J. Chem. 32 (2008) 705.

[55] K. S. Low, J. M. Cole, X. Zhou, N. Yufa, Acta Crystallogr. B 68 (2012) 137.

[56] Y. Harima, K. Kawabuchi, S. Kajihara, A. Ishii, Y. Ooyama, K. Takeda, Appl. Phys. Lett. 90 (2007) 103517.

[57] P. K. D. D. P. Pitigala, M. K. I. Senevirathna, V. P. S. Perera, K. Tennakone, Compt. Rend. Chim. 9 (2006) 605.

[58] P. V. V. Jayaweera, A. G. U. Perera, M. K. I. Senevirathna, P. K. D. D. P. Pitigala, K. Tennakone, Appl. Phys. Lett. 85 (2004) 5754.

[59] T. Daeneke, A. J. Mozer, T.-H. Kwon, N. W. Duffy, A. B. Holmes, U. Bach, L. Spiccia, Energy Environ. Sci. 5 (2012) 7090.

[60] T. Daeneke, T.-H. Kwon, A. B. Holmes, N. W. Duffy, U. Bach and L. Spiccia, Nature Chem. 3 (2011) 211.

[61] S. M. Feldt, U. B. Cappel, E. M. J. Johansson, G. Boschloo, A. Hagfeldt, J. Phys. Chem. C 114 (2010) 10551.

[62] B. A. Gregg, F. Pichot, S. Ferrere, C. L. Fields, J. Phys. Chem. B. 105 (2001) 1422.

[63] A. Kumar, R. Chauhan, K. C. Molloy, G. Kociok-Köhn, L. Bahadur, N. Singh, Chem. Eur. J. 16 (2010) 4307.

[64] R. Chauhan, M. Trivedi, L. Bahadur, A. Kumar, Chem. Asian J. 6 (2011) 1525.

[65] S. K. Singh, R. Chauhan, B. Singh, K. Diwan, G. Kociok-Köhn, L. Bahadur, N. Singh, Dalton Trans. 41 (2012) 1373.

[66] V. Singh, R. Chauhan, A. Kumar, L. Bahadur and N. Singh, Dalton Trans. 39 (2010) 9779.

[67] S. Appleyard, Renewable Energy 34 (2009) 1651.

[68] T. Daeneke, Y. Uemura, N. W. Duffy, A. J. Mozer, N. Koumura, U. Bach, L. Spiccia, Adv. Mater. 24 (2012) 1222.

[69] I. A. Rutkowska, A. Andrearczyk, S. Zoladek, M. Goral, K. Darowicki, P. J. Kulesza, J. Solid State Electrochem. 15 (2011) 2545.

[70] H. Nusbaumer, S. M. Zakeeruddin, J.-E. Moser, M. Grätzel, Chem. Eur. J. 9 (2003) 3756.

[71] T. W. Hamann, Dalton Trans. 41 (2012) 3111.

[72] S. M. Feldt, E. A. Gibson, E. Gabrielsson, L. Sun, G. Boschloo, A. Hagfeldt, J. Am. Chem. Soc. 132 (2010) 16714.

[73] F. Odobel, Y. Pellegrin, E. A. Gibson, A. Hagfeldt, A. L. Smeigh, L. Hammarström, Coord. Chem. Rev. 256 (2012) 2414.

[74] C. L. Linfoot, P. Richardson, K. L. McCall, J. R. Durrant, A. Morandeira, N. Robertson, Solar Energy 85 (2011) 1195.

[75] Q. Miao, J. Gao, Z. Wang, H. Yu,Y. Luo, T. Ma, Inorg. Chim. Acta 376 (2011) 619.

[76] S. Dalgleish, N. Robertson, Chem. Commun. (2009) 5826.

[77] S. Dalgleish, J. G. Labram, Z. Li, J. Wang, C. R. McNeill, T. D. Anthopoulos, N. C. Greenham, N. Robertson, J. Mater. Chem. 21 (2011) 15422.

[78] J. Deng, L. Guo, Q. Xiu, L. Zhang, G. Wen and C. Zhong, Mater. Chem. Phys. 133 (2012), 452.

[79] L. Guo, J. Deng, L. Zhang, Q. Xiu, G. Wen, C. Zhong, Dyes Pigments 92 (2012) 1062.

[80] J. Deng, Q. Xiu, L. Guo, L. Zhang, G. Wen, C. Zhong, J. Mater. Sci., 47 (2012) 3383.

[81] S. Kushwaha, L. Bahadur, Int. J. Photoenergy (2011) article 980560.

[82] N. Robertson, ChemSusChem 1 (2008) 977.

[83] N. Alonso-Vante, J-F. Nierengarten, J.-P. Sauvage, J. Chem. Soc. Dalton Trans. (1994) 1650.

[84] N. Armaroli, Chem. Soc. Rev. 30 (2001) 113.

[85] N. Armaroli, Top. Curr. Chem. 280 (2007) 69.

[86] X. Lu, C.-M. L. Wu, S. Wei, W. Guo, J. Phys. Chem. A 114 (2010) 1178.

[87] X. Lu, S. Wei, C.-M. L. Wu, S. Li, W. Guo, J. Phys. Chem. C 115 (2011) 3753.

[88] J. Baldenebro-López, J. Castorena-González, N. Flores-Holguín, J. Almaral-Sánchez, D. Glossman-Mitnik, Int. J. Mol. Sci. 13 (2012) 16005.

[89] M. W. Mara, N. E. Jackson, J. Huang, A. B. Stickrath, X. Zhang, N. A. Gothard, M. A. Ratner, L. X. Chen,

[90] S. Sakaki, T. Kuroki, T. Hamada, J. Chem. Soc., Dalton Trans. (2002) 840.

[91] T. Bessho, E. C. Constable, M. Grätzel, A. Hernandez Redondo, C. E. Housecroft, W. Kylberg, Md. K. Nazeeruddin, M. Neuburger, S. Schaffner, Chem. Commun. (2008) 3717.

[92] E. C. Constable, A. Hernandez Redondo, C. E. Housecroft, M. Neuburger, S. Schaffner, Dalton Trans. (2009) 6634.

[93] A. Hernandez Redondo, E. C. Constable, C. E. Housecroft, Chimia 63 (2009) 205.

[94] B. Bozic-Weber, E. C. Constable, C. E. Housecroft, M. Neuburger and J. R. Price, Dalton Trans. 39 (2010) 3585.

[95] B. Bozic-Weber, S. Y. Brauchli, E. C. Constable, S. O. Fürer, C. E. Housecroft, I. A. Wright, Phys. Chem. Chem. Phys. 15 (2013) 4500.

[96] B. Bozic-Weber, E. C. Constable, C. E. Housecroft, P. Kopecky, M. Neuburger, J. A. Zampese, Dalton Trans. 40 (2011) 12584.

[97] B. Bozic-Weber, V. Chaurin, E. C. Constable, C. E. Housecroft, M. Meuwly, M. Neuburger, J. A. Rudd, E. Schönhofer, L. Siegfried, Dalton Trans. 41 (2012) 14157.

[98] L. N. Ashbrook, C. M. Elliott, J. Phys. Chem. C 117 (2013) 3853.

[99] Y.-J. Yuan, Z.-T. Yu, J.-Y. Zhang, Z.-G. Zou, Dalton Trans. 41 (2012) 9594.

[100] J. A. Treadway, B. Loeb, R. Lopez, P. A. Anderson, F. R. Keene, T. J. Meyer, Inorg. Chem. 35 (1996) 2242.

[101] C. L. Linfoot, P. Richardson, T. E. Hewat, O. Moudam, M. M. Forde, A. Collins, F. White, N. Robertson, Dalton Trans. 39 (2010) 8945.

[102] K. L. McCall, J. R. Jennings, H. Wang, A. Morandeira, L. M. Peter, J. R. Durrant, L. J. Yellowlees, N. Robertson, Eur. J. Inorg. Chem. (2011) 589.

[103] Y. Kim, J. H. Jeong, M. Kang, Inorg. Chim. Acta 365 (2011) 400.

[104] L. Xiao, Y. Liu, Q. Xiu, L. Zhang, L. Guo, H. Zhang, C. Zhong, Tetrahedron 66 (2010) 2835.

[105] G. Wen, L. Zhang, L. Guo, Q. Xiu, J. Deng, C. Zhong, Polym. Int. 61 (2012) 1016.

[106] B. Bozic-Weber, E. C. Constable, N. Hostettler, C. E. Housecroft, R. Schmitt, E. Schönhofer, Chem. Commun. 48 (2012) 5727.

[107] L. Zhang, Y. Yang, R. Fan, P. Wang, L. Li, Dyes Pigments 92 (2012) 1314.